

Microscopic theory of glassy dynamics and glass transition for molecular crystals

Michael Ricker* and Rolf Schilling†

Institut für Physik, Johannes Gutenberg-Universität Mainz, Staudinger Weg 7, D-55099 Mainz, Germany

(Dated: February 15, 2017)

We derive a microscopic equation of motion for the dynamical orientational correlators of molecular crystals. Our approach is based upon mode coupling theory. Compared to liquids we find four main differences: (i) the memory kernel contains Umklapp processes if the total momentum of two orientational modes is outside the first Brillouin zone, (ii) besides the static two-molecule orientational correlators one also needs the static one-molecule orientational density as an input, where the latter is nontrivial due to the crystal's anisotropy, (iii) the static orientational current density correlator does contribute an anisotropic, inertia-independent part to the memory kernel, (iv) if the molecules are assumed to be fixed on a rigid lattice, the tensorial orientational correlators and the memory kernel have vanishing $l, l' = 0$ components, due to the absence of translational motion. The resulting mode coupling equations are solved for hard ellipsoids of revolution on a rigid sc-lattice. Using the static orientational correlators from Percus-Yevick theory we find an ideal glass transition generated due to precursors of orientational order which depend on X_0 and φ , the aspect ratio and packing fraction of the ellipsoids. The glass formation of oblate ellipsoids is enhanced compared to that for prolate ones. For oblate ellipsoids with $X_0 \lesssim 0.7$ and prolate ellipsoids with $X_0 \gtrsim 4$, the critical diagonal nonergodicity parameters in reciprocal space exhibit more or less sharp maxima at the zone center with very small values elsewhere, while for prolate ellipsoids with $2 \lesssim X_0 \lesssim 2.5$ we have maxima at the zone edge. The off-diagonal nonergodicity parameters are not restricted to positive values and show similar behavior. For $0.7 \lesssim X_0 \lesssim 2$, no glass transition is found because of too small static orientational correlators. In the glass phase, the nonergodicity parameters show a much more pronounced \mathbf{q} -dependence.

PACS numbers: 61.43.-j, 64.70.Pf, 63.90.+t

I. INTRODUCTION

The experimental and theoretical investigation of systems with *self-generated* disorder has mainly been devoted to simple and molecular liquids [1, 2]. In their supercooled state at low temperatures or high densities, liquids exhibit nontrivial dynamics, often called glassy dynamics. Decreasing the temperature T or increasing the number density n may result in a glass transition. The physical origin of glassy dynamics and the glass transition is the formation of a cage by the particles. For not too low temperatures and not too high densities, the cage's lifetime is finite, i.e. a particle can escape with a finite probability. However, if the lifetime diverges, e.g. at a critical temperature, the particles remain localized in their cages. In that case an ideal glass transition occurs at that temperature.

There is no general agreement about the theoretical description of the glass transition. From a practical point of view one often considers the so-called calorimetric glass transition temperature T_g as the temperature at which a supercooled liquid becomes a structural glass. But T_g depends on the cooling process. Therefore, it is not well defined. Besides T_g , there exist two better defined characteristic temperatures, which are T_c , the mode coupling transition temperature, and T_K , the Kauzmann temper-

ature. At T_K the excess entropy of a supercooled liquid with respect to its crystalline phase disappears. This is a very old concept which only recently has been put onto a microscopic basis by the replica theory for structural glasses (see [3] and references therein). The existence of a purely dynamical glass transition at a critical temperature T_c has been suggested about two decades ago [4]. This approach is based on mode coupling theory (MCT). MCT describes the cage effect (as explained above) in a self-consistent way. At T_c a transition from an ergodic to a nonergodic phase occurs. Close to T_c the relaxational dynamics of e.g. the density fluctuations, exhibits two time scaling laws with relaxation times which diverge at T_c . For more details and comparison of the MCT predictions with experimental and simulational results the reader is referred to Refs. [5, 6, 7, 8, 9]. A review of MCT, replica theory of structural glasses and a selection of phenomenological theories is given in Ref. [10].

Glassy behavior of systems with self-generated disorder is not restricted to liquids. There exist so-called molecular crystals [11] where molecules are located at sites of a periodic lattice. At higher temperatures their orientational degrees of freedom (ODOF) may be dynamically disordered, i.e. ergodic. This phase is called the plastically crystalline phase [12]. Decreasing temperature lowers the lattice constants which in turn leads to an increase of the steric hindrance between the ODOF. This may result in the formation of an "orientational" cage in which the orientation of a molecule is captured on a certain time scale, quite similar to liquids. If this time scale diverges the plastic crystal undergoes an ideal orientational glass tran-

*Electronic address: mricker@uni-mainz.de

†Electronic address: rschill@uni-mainz.de

sition. The corresponding phase is called *glassy crystal*. That such a glass transition really occurs has been proven experimentally several decades ago. First systematic experimental indication for the formation of glassy crystals has been given in 1974 for several molecular crystals [13]. Since then a lot of glassy crystals were found. Without claiming completeness the most intensively studied molecular crystals are cyanoadamantane [14, 15, 16, 17], chloradamantane [18] and ethanol [19, 20]. Ethanol has the big advantage that it can form either a supercooled liquid, a structural glass, a plastic crystal, a glassy crystal and an orientationally ordered crystal within a small temperature interval around 100 K. Therefore, it has been investigated experimentally to explore the role of translational degrees of freedom (TDOF) and ODOF for glassy behavior [20]. These experiments have shown that the ODOF of molecular crystals exhibit quite similar glassy behavior than conventional supercooled liquids. Additionally, comparing different molecular crystals with each other, similar glassy behavior was found [15]. These similarities also include dynamical heterogeneities [21]. The largest deviations of molecular crystals from supercooled liquids were observed in dielectric spectroscopy. The former exhibit a rather weak excess wing, or even no such wing, in contrast to supercooled liquids [15].

An interesting model for molecular crystals has been studied some years ago. The molecules were approximated by infinitely thin hard rods with length L which were either fixed with their centers on a fcc-lattice [22] or with their endpoints on a sc-lattice [23]. MD- [22] and MC-simulations [23], respectively, have shown the existence of glasslike dynamics. Particularly a critical length $l_c = L/a$ (a is the lattice constant) has been determined at which an orientational glass transition occurs [22, 23]. However, this transition is not sharp, in close analogy to supercooled liquids. The system of infinitely thin hard rods is particularly interesting since there are *no* static orientational correlations. Consequently, glassy behavior does not originate from growing static correlations, but results from *entanglement* which leads to a “dynamical cage”.

As far as we know there is no *microscopic* theory which describes glassy behavior of molecular crystals with self-generated disorder. For mixed crystals [24], i.e. crystals with *quenched disorder*, a microscopic theory for the glass transition has been worked out [25]. This theory is based on MCT and takes into account ODOF and TDOF, i.e. lattice displacements, as well as translation-rotation [26] coupling. The displacements are crucial, since the statistical substitution, of e.g. CN molecules in KCN by Br atoms, leading to the well-known mixed crystal compound $(\text{KBr})_{1-x}(\text{KCN})_x$ [24], generates random displacements. Due to the translation-rotation coupling, these random displacements induce random fields acting on the ODOF. MCT was also applied to spin glass models, where the coupling constants between spins are at random [27]. Unfortunately, the quality of MCT predictions for mixed crystals and spin glasses has not

really been tested, in contrast to supercooled liquids [5, 6, 7, 8, 9].

Since MCT has been very successful [5, 6, 7, 8, 9] to describe glassy dynamics of supercooled liquids, and since it has also been applied to mixed crystals and spin glasses, it is natural to derive MCT equations for plastic crystals, as well. This will be done in Sec. II. The calculation of the glass transition line and the critical nonergodicity parameters from the MCT equations will be presented in Sec. III for hard ellipsoids on a sc-lattice. The final section contains a discussion of the results and some conclusions. More technical details are put into four appendices.

II. THEORETICAL FRAMEWORK

In this section we will describe how MCT equations can be derived for molecular crystals. The strategy is quite similar to that for simple liquids [5, 6], molecular liquids of linear molecules [28, 29] and arbitrary molecules [30]. The introduction of the microscopic orientational density, the corresponding current density and their time-dependent correlators will be described in subsection II A. Then, in subsection II B, we apply the Mori-Zwanzig projection formalism [31, 32] to derive an equation of motion for the time-dependent orientational correlators. Following MCT for liquids, the memory kernel is then approximated by a bilinear superposition of the time-dependent orientational correlators.

A. Microscopic orientational densities and their correlators

We consider a Bravais lattice with N lattice sites. Since the experimental and simulational results for supercooled molecular crystals [14, 15, 16, 17, 18, 19, 20, 21] have demonstrated that glassy behavior can occur due to steric hindrance of the ODOF, we restrict ourselves to a *rigid* lattice, i.e. we neglect the translation-rotation coupling. Then, the increase of steric hindrance by decreasing temperature can be accounted for by either a variation of the lattice constant or equivalently by an increase of the size of the molecules. At each lattice site we fix a molecule. The natural way is to fix its center of mass. All molecules are assumed to be identical and rigid, as well. We will consider *linear* molecules only. Generalization to *arbitrary* molecules can be performed like for molecular liquids [30].

It is also obvious that the ODOF are best described in a molecule-fixed frame with its origin coinciding with the lattice site. In principle one could choose any other reference point [29]. But this would *artificially* introduce TDOF, besides the ODOF. Using the former choice, the ODOF of the n -th molecule at the site with lattice vector \mathbf{x}_n is given by the angles $\Omega_n = (\theta_n, \phi_n)$. The third angle χ_n with respect to the symmetry axis is irrelevant

for the glassy dynamics. The moment of inertia for the axes perpendicular to the symmetry axis is denoted by I . The interaction between the molecules is given by $V(\Omega_1, \dots, \Omega_N)$ and the classical dynamics follows from the classical Hamiltonian

$$\begin{aligned} H(\{\theta_n, \phi_n\}, \{p_{\theta_n}, p_{\phi_n}\}) &= \\ &= \frac{1}{2I} \sum_{n=1}^N \left[p_{\theta_n}^2 + \frac{p_{\phi_n}^2}{\sin^2 \theta_n} \right] + V(\{\theta_n, \phi_n\}), \end{aligned} \quad (1)$$

where p_{θ_n} and p_{ϕ_n} are the momenta conjugate to θ_n and ϕ_n , respectively.

Next we introduce the microscopic, local orientational density

$$\rho_n(\Omega, t) = \delta(\Omega | \Omega_n(t)), \quad (2)$$

with $\delta(\Omega | \Omega') = (\sin \theta)^{-1} \delta(\theta - \theta') \delta(\phi - \phi')$ and $\Omega_n(t)$ the classical trajectory of the n -th molecule. The one-molecule orientational density $\rho^{(1)}(\Omega)$ is given by

$$\rho^{(1)}(\Omega) = \langle \delta(\Omega | \Omega_n(t)) \rangle, \quad (3)$$

which is independent on t and, for identical molecules, also on n . $\langle (\cdot) \rangle$ denotes canonical averaging with respect to initial conditions in the $4N$ -dimensional phase space.

Taking the time derivative of $\rho_n(\Omega, t)$ leads to the continuity equation.

$$\dot{\rho}_n(\Omega, t) = i \hat{\mathbf{L}}_{\Omega_n} \cdot \mathbf{j}_n(\Omega, t). \quad (4)$$

Here, $\hat{\mathbf{L}}_{\Omega_n}$ is the angular momentum operator acting on Ω_n , and

$$\mathbf{j}_n(\Omega, t) = \boldsymbol{\omega}_n(t) \delta(\Omega | \Omega_n(t)) \equiv \boldsymbol{\omega}_n(t) \rho_n(\Omega, t) \quad (5)$$

is the corresponding orientational current density, which involves the angular velocity $\boldsymbol{\omega}_n(t)$. We also introduce the ‘‘longitudinal’’ orientational current density

$$j_n(\Omega, t) = \hat{\mathbf{L}}_{\Omega_n} \cdot \mathbf{j}_n(\Omega, t). \quad (6)$$

With these quantities we can define the time-dependent orientational correlators:

$$G_{nn'}(\Omega, \Omega', t) = \langle \delta\rho_n(\Omega, t) \delta\rho_{n'}(\Omega') \rangle \quad (7)$$

of the local orientational density fluctuations

$$\delta\rho_n(\Omega, t) = \rho_n(\Omega, t) - \langle \rho_n(\Omega, t) \rangle = \rho_n(\Omega, t) - \rho^{(1)}(\Omega), \quad (8)$$

as well as

$$J_{nn'}(\Omega, \Omega', t) = 4\pi \langle j_n(\Omega, t) j_{n'}(\Omega') \rangle. \quad (9)$$

Here, $\delta\rho_n(\Omega) \equiv \delta\rho_n(\Omega, 0)$ and $j_n(\Omega) \equiv j_n(\Omega, 0)$.

Similar to molecular liquids [28, 29], we expand the orientation-dependent functions with respect to spherical harmonics $Y_\lambda(\Omega)$, $\lambda = (lm)$, as already done for

the static correlators [33][51]. This allows to represent any functions $f_n(\Omega, t)$ and $F_{nn'}(\Omega, \Omega', t)$ by their λ - and Fourier-transforms. The corresponding transform of $G_{nn'}(\Omega, \Omega', t)$ leads to the intermediate scattering functions

$$S_{\lambda\lambda'}(\mathbf{q}, t) = \frac{4\pi}{N} \langle \delta\rho_\lambda^*(\mathbf{q}, t) \delta\rho_{\lambda'}(\mathbf{q}) \rangle \quad (10)$$

and the corresponding current density correlators

$$J_{\lambda\lambda'}(\mathbf{q}, t) = \frac{4\pi}{N} \langle j_\lambda^*(\mathbf{q}, t) j_{\lambda'}(\mathbf{q}) \rangle. \quad (11)$$

These correlators form matrices $\mathbf{S}(\mathbf{q}, t) = (S_{\lambda\lambda'}(\mathbf{q}, t))$, etc. The wave vectors \mathbf{q} are restricted to the 1. Brillouin zone (1.BZ), due to the lattice translational invariance. The correlators $S_{\lambda\lambda'}(\mathbf{q}, t)$ form a complete set. For example the neutron scattering function $S_{\text{neutron}}(\mathbf{q}, t)$ can be expressed by $\{S_{\lambda\lambda'}(\mathbf{q}, t)\}$ using the scattering lengths of the molecular sites [36].

Note that the correlators (10) and (11) vanish for $l = 0$ and/or $l' = 0$, due to the absence of TDOF. The symmetries of the orientational correlators discussed in Ref. [33] also hold for the time dependent quantities. They will be applied to reduce the number of independent correlators.

B. Mode coupling theory

The goal of this subsection is to derive an approximate equation of motion for the intermediate scattering functions $S_{\lambda\lambda'}(\mathbf{q}, t)$ of molecular crystals. Due to the rigid lattice, only ODOF are involved. In case that the steric hindrance is large enough the orientational density fluctuations $\delta\rho_\lambda(\mathbf{q}, t)$ contain slow parts. Choosing $\delta\rho_\lambda(\mathbf{q}, t)$ and the ‘‘longitudinal’’ current density $j_\lambda(\mathbf{q}, t)$ as slow variables, we can apply the Mori-Zwanzig formalism [31, 32] to derive an equation of motion for $\mathbf{S}(\mathbf{q}, t)$:

$$\begin{aligned} \ddot{\mathbf{S}}(\mathbf{q}, t) + \mathbf{J} \mathbf{S}^{-1}(\mathbf{q}) \dot{\mathbf{S}}(\mathbf{q}, t) + \\ + \int_0^t dt' \mathbf{M}(\mathbf{q}, t-t') \mathbf{J}^{-1} \dot{\mathbf{S}}(\mathbf{q}, t') = \mathbf{0}. \end{aligned} \quad (12)$$

The notation $^{-1}$ means the inverse of the $l, l' > 0$ block of the respective matrix, i.e. the inverse with respect to the subspace of non-constant functions in angular space. This is because the first rows and columns of these matrices vanish. The only exception from this rule is \mathbf{d}^{-1} in App. D. The prefactor $\mathbf{J} \mathbf{S}^{-1}(\mathbf{q})$ in Eq. (12) is related to

$$\boldsymbol{\Omega}^2(\mathbf{q}) = \mathbf{S}^{-1/2}(\mathbf{q}) \mathbf{J} \mathbf{S}^{-1/2}(\mathbf{q}), \quad (13)$$

which is the square of the symmetric microscopic frequency matrix ($\Omega_{\lambda\lambda'}(\mathbf{q})$). It depends on the static orientational correlators $\mathbf{S}(\mathbf{q})$ and on $\mathbf{J} \equiv (J_{\lambda\lambda'}(\mathbf{q}))$, which is

independent of \mathbf{q} (see App. A). The matrix elements of the memory kernel $\mathbf{M}(\mathbf{q}, t)$ are given by

$$M_{\lambda\lambda'}(\mathbf{q}, t) = \frac{4\pi}{N} \langle (\mathcal{L} j_\lambda(\mathbf{q}))^* | Q e^{-iQ\mathcal{L}Qt} Q | \mathcal{L} j_{\lambda'}(\mathbf{q}) \rangle, \quad (14)$$

the correlations of the fluctuating forces $Q | \mathcal{L} j_\lambda(\mathbf{q}) \rangle$. \mathcal{L} is the Liouville operator and $Q = 1 - P_\rho - P_j$ (see Eq. (B3)) projects perpendicular to the slow variables $\delta\rho_\lambda(\mathbf{q})$ and $j_\lambda(\mathbf{q})$.

In a final step we perform the mode coupling approximation for the slow part $\mathbf{m}(\mathbf{q}, t)$ of $\mathbf{J}^{-1} \mathbf{M}(\mathbf{q}, t) \mathbf{J}^{-1}$, which enters Eq. (23), yielding (see Appendices B-D)

$$m_{\lambda\lambda'}(\mathbf{q}, t) \approx \frac{1}{2N} \sum_{\mathbf{Q}} \sum'_{\substack{\mathbf{q}_1, \mathbf{q}_2 \\ \in 1.\text{BZ}}} \sum'_{\lambda_1 \lambda'_1 \lambda_2 \lambda'_2} V(\mathbf{q}\lambda\lambda' | \mathbf{q}_1 \lambda_1 \lambda'_1; \mathbf{q}_2 \lambda_2 \lambda'_2) S_{\lambda_1 \lambda'_1}(\mathbf{q}_1, t) S_{\lambda_2 \lambda'_2}(\mathbf{q}_2, t). \quad (15)$$

The vertices are

$$\begin{aligned} V(\mathbf{q}\lambda\lambda' | \mathbf{q}_1 \lambda_1 \lambda'_1; \mathbf{q}_2 \lambda_2 \lambda'_2) &= \\ &= \frac{1}{(4\pi)^2} \sum'_{\lambda_3 \lambda'_3} (\tilde{\mathbf{J}}^{-1})_{\lambda\lambda_3} \left[\sum'_{\lambda''} v(\mathbf{q}\lambda_3 | \mathbf{q}_1 \lambda_1; \mathbf{q}_2 \lambda_2; \lambda'') \right] \times \\ &\times \left[\sum'_{\lambda''' } v(\mathbf{q}\lambda'_3 | \mathbf{q}_1 \lambda'_1; \mathbf{q}_2 \lambda'_2; \lambda''') \right]^* (\tilde{\mathbf{J}}^{-1})_{\lambda'_3 \lambda'} , \end{aligned} \quad (16)$$

where

$$\begin{aligned} v(\mathbf{q}\lambda | \mathbf{q}_1 \lambda_1; \mathbf{q}_2 \lambda_2; \lambda'') &= \\ &= b(l''l_2l) C(l''l_2l, m''m_2m) c_{\lambda\lambda_1}(\mathbf{q}_1) + (1 \leftrightarrow 2), \end{aligned} \quad (17)$$

$$\begin{aligned} b(l'l''') &= \frac{1}{2} i^{l+l''-l'''} \left[\frac{(2l+1)(2l'+1)}{2l''+1} \right]^{\frac{1}{2}} \times \\ &\times \left[1 + (-1)^{l+l''+l'''} \right] \sqrt{l(l+1)} \sqrt{l''(l''+1)} C(l'l''', 101), \end{aligned} \quad (18)$$

and

$$\tilde{J}_{\lambda\lambda'} = \frac{I}{kT} J_{\lambda\lambda'}, \quad (19)$$

is the inertia and temperature-independent part of $J_{\lambda\lambda'}$. $\sum'_{\mathbf{q}_1, \mathbf{q}_2}$ denotes summation such that $\mathbf{q}_1 + \mathbf{q}_2 = \mathbf{q} + \mathbf{Q}$, with \mathbf{Q} a reciprocal lattice vector, and \sum'_{λ} indicates summation over all $\lambda \neq (00)$. $C(l'l'', mm'm'')$ are the Clebsch-Gordon coefficients and $c_{\lambda\lambda'}(\mathbf{q})$ the direct correlation function matrix elements.

The result, Eqs. (15)-(19), has a striking similarity to the slow rotational part $m_{\lambda\lambda'}^{\text{RR}}(\mathbf{q}, t)$ of the memory kernel for molecular liquids [28, 29]. This is not surprising. Particularly $v(\mathbf{q}\lambda | \mathbf{q}_1 \lambda_1; \mathbf{q}_2 \lambda_2; \lambda'')$ are identical, up to a

factor $\sqrt{l(l+1)}$. This similarity originates from the factorization of a static three-point correlator described in Appendix D. It is this approximation which leads to the rather simple result, Eqs. (16) and (17), for the vertices. Of course, taking the static three-point correlator from a simulation would make this factorization approximation unnecessary. However, we do not expect any qualitative influence using our approximation instead of the correct simulational result. Such an influence is only to be expected for systems which interact through three-, four-... body potentials. Since the molecules are fixed on lattice sites, such covalent bonds may be less important for molecular crystals.

There are four main differences with respect to MCT for molecular liquids. First, the tensorial MCT equations for molecular liquids are first order integro-differential equations which can not be transformed to a second order integro-differential equation, like Eq. (12). Second, for molecular crystals $m_{\lambda\lambda'}(\mathbf{q}, t)$ contains a sum over reciprocal lattice vectors \mathbf{Q} . Therefore, the sum over $\mathbf{q}_1, \mathbf{q}_2$ involves *Umklapp* processes. Third, due to the rigid lattice, only the $l, l' > 0$ matrix elements are nonzero. Fourth, the static current density correlator $J_{\lambda\lambda'}$ in Eq. (15) does not cancel completely, as it does for a molecular liquid. There remains an anisotropic part $\tilde{J}_{\lambda\lambda'}$, which equals $l(l+1)\delta_{\lambda\lambda'}$ for a liquid and is defined in Eq. (19). $\tilde{J}_{\lambda\lambda'}$ can be related to the λ -transform $\rho_\lambda^{(1)}$ of the one-molecule orientational density $\rho^{(1)}(\Omega)$, which is needed as an input (for details see App. A).

There is no explicit dependence of the kernel $\mathbf{m}(\mathbf{q}, t)$ on T and I . On a large time scale we can neglect $\ddot{\mathbf{S}}(\mathbf{q}, t)$ in Eq. (12). The remaining equation does not involve any inertia effect, i.e. the glassy dynamics depends not on I , except for fixing the time scale.

The vertices $V(\mathbf{q}\lambda\lambda' | \mathbf{q}_1 \lambda_1 \lambda'_1; \mathbf{q}_2 \lambda_2 \lambda'_2)$ depend on $\tilde{\mathbf{J}}$ and the direct correlation function $\mathbf{c}(\mathbf{q})$ only, where $\mathbf{c}(\mathbf{q})$ is related to the *static* orientational correlators $\mathbf{S}(\mathbf{q})$ by the Ornstein-Zernike (OZ) equation for molecular crystals [33]:

$$\mathbf{S}(\mathbf{q}) = \left[\mathbf{D}^{-1} - \frac{1}{4\pi} \mathbf{c}(\mathbf{q}) \right]^{-1}. \quad (20)$$

This equation is similar to that for molecular liquids [28, 37][52], with exception of the appearance of \mathbf{D} . $D_{\lambda\lambda'}$ is the λ -transform of $D(\Omega, \Omega') = 4\pi [\rho^{(1)}(\Omega) \delta(\Omega|\Omega') - \rho^{(1)}(\Omega) \rho^{(1)}(\Omega')]$ and can be expressed by the λ -transform of $\rho^{(1)}(\Omega)$, too.

This discussion makes clear that the closed set of MCT equations (12)-(19) requires two different *static* input quantities, the one-molecule quantities $D_{\lambda\lambda'}$, $\tilde{J}_{\lambda\lambda'}$ which can be expressed by $\{\rho_\lambda^{(1)}\}$ and the two-molecule correlators $S_{\lambda\lambda'}(\mathbf{q})$, or $c_{\lambda\lambda'}(\mathbf{q})$. Note also that we have neglected contributions to $m_{\lambda\lambda'}(\mathbf{q}, t)$ coming from the fast part of $\delta\rho(\mathbf{q}, t)$ which leads to a damping term in Eq. (12). On a long time scale this has no influence.

Here we restrict ourselves to the investigation of the orientational glass transition itself. For this we introduce

the nonergodicity parameters (NEP, not normalized!)

$$F_{\lambda\lambda'}(\mathbf{q}) = \lim_{t \rightarrow \infty} S_{\lambda\lambda'}(\mathbf{q}, t). \quad (21)$$

In the limit $t \rightarrow \infty$, Eq. (12) leads to

$$\mathbf{S}^{-1}(\mathbf{q}) \mathbf{F}(\mathbf{q}) [\mathbf{S}(\mathbf{q}) - \mathbf{F}(\mathbf{q})]^{-1} = \mathcal{F}[\mathbf{F}(\mathbf{q})] \quad (22)$$

where

$$\mathcal{F}[\mathbf{F}(\mathbf{q})] = \lim_{t \rightarrow \infty} \mathbf{m}(\mathbf{q}, t). \quad (23)$$

Eqs. (22) and (23) are matrix equations for $l, l' > 0$, since the first columns and rows of the involved matrices vanish, due to the rigid lattice.

III. RESULTS FOR HARD ELLIPSOIDS

After having derived equations of motion for the orientational correlators $S_{\lambda\lambda'}(\mathbf{q}, t)$, their time dependence could be calculated numerically. Although the mathematical structure of the MCT-equations (12), (15)-(19) is identical to that of more-component liquids, the numerical solution is hampered due to the *anisotropy* of the lattice, in contrast to liquids. Because of this anisotropy the correlators also depend on the direction of \mathbf{q} . For liquids it has turned out that the restriction to several hundreds of values for $q = |\mathbf{q}|$ leads to rather precise solutions of the MCT-equations. We will see below that we have to choose several thousands of \mathbf{q} vectors within the first Brillouin zone. In addition, in comparison to molecular liquids, there are more independent correlators for each pair (l, l') , increasing the number of equations even more. Consequently, a numerical solution will require either an improvement of the numerical code [38] usually used for the numerical solution of the MCT-equations and/or further simplification of $S_{\lambda\lambda'}(\mathbf{q})$, e.g. neglecting the dependence on $\mathbf{q}/|\mathbf{q}|$. Since we want to avoid such type of approximations we will restrict ourselves to the calculation of the glass transition point and the corresponding critical nonergodicity parameters and leave the solution of the time-dependent equations for future. Nevertheless, their identical structure to that of liquids already ensures the validity of, e.g., the two time scaling laws [5] for molecular crystals as well.

In order to solve Eq. (22) we have chosen hard ellipsoids of revolution, fixed with their centers on a sc-lattice with lattice constant equal to one. The symmetry axis of the ellipsoids has length a and the length of the perpendicular axes is b . Replacing linear, rigid molecules by hard ellipsoids is probably not a bad approximation since the steric hindrance is qualitatively the same. In addition, the choice of hard ellipsoids has two advantages: First, we have already calculated the static orientational correlators $S_{\lambda\lambda'}(\mathbf{q})$ for $l, l' \leq 4$ within the Percus-Yevick (PY) approximation, and $\rho_\lambda^{(1)}$ (which yields $\tilde{J}_{\lambda\lambda'}$ and $D_{\lambda\lambda'}$) for $l \leq 8$ by MC-simulations. Second, we have

recently solved the MCT-equations for a molecular *liquid* of hard ellipsoids [39] which allows to compare the conditions for the appearance of the ideal glass transition for the ellipsoids on a lattice and in their liquid phase. This comparison will allow to estimate the qualitative or quantitative role of TDOF for the freezing of the ODOF. Furthermore, the ellipsoids' head-tail symmetry leads to a decomposition of Eq. (12) and therefore of Eq. (22) into a closed set of equations for $S_{\lambda\lambda'}(\mathbf{q}, t)$ and $F_{\lambda\lambda'}(\mathbf{q})$, respectively, for l, l' both even and a set of these quantities for l, l' both odd. All correlators with l even and l' odd or vice versa are zero. The set of equations for l, l' both even is closed because the memory kernel only contains correlators with l and l' even. This is in contrast to the equations for l, l' odd. The corresponding memory kernel contains a bilinear coupling of correlators with l, l' even with those where l, l' are odd. It is easy to prove that

$$S_{\lambda\lambda'}^{(s)}(t) \equiv S_{\lambda\lambda'}(\mathbf{q}, t), \quad (24)$$

for l, l' both odd. The “self” correlator $S_{\lambda\lambda'}^{(s)}(t)$ is the λ -transform of $G_{nn}(\Omega, \Omega', t)$, up to a prefactor. In contrast to this the “self” correlator with l, l' even is given by

$$S_{\lambda\lambda'}^{(s)}(t) = \frac{1}{N} \sum_{\mathbf{q} \in 1.\text{BZ}} S_{\lambda\lambda'}(\mathbf{q}, t). \quad (25)$$

Similar relations hold for the NEP.

There is a technical disadvantage connected with the hard body potential between the ellipsoids. The inversion of the static correlators, occurring e.g. in the projectors (cf. Eq.(14)) and vertices (cf. Eq. (16)), needs some caution. Readers interested in this point are referred to Refs. [33, 40]. We stress that the second paper cited in Ref. [33] and [40] contain additional technical information, particularly the discussion of those mathematical problems related to hard core interactions. However, these details will not be needed in the following.

The numerical solution of Eqs. (22), (23) requires a restriction of the matrices to $l, l' \leq l_{\max}$. We have chosen $l_{\max} = 4$. The \mathbf{q} -vectors are discretized, i.e. for the α -component of \mathbf{q} we have chosen $q_\alpha = \nu_\alpha \frac{2\pi}{M}$, $\nu_\alpha = -\frac{M}{2}, -\frac{M}{2} + 1, \dots, 0, \dots, \frac{M}{2} - 1$ with $M = 32$, which makes a total of 32768 \mathbf{q} -vectors. Due to the point symmetry of the lattice, the number of independent $F_{\lambda\lambda'}(\mathbf{q})$ can be reduced. For more details the reader is referred to Refs. [33, 40]. The solution of Eqs. (22) yields the NEP $F_{\lambda\lambda'}(\mathbf{q})$ and the corresponding normalized quantities $f_{\lambda\lambda'}(\mathbf{q})$, where the normalization $f_{\lambda\lambda'}(\mathbf{q}) = F_{\lambda\lambda'}(\mathbf{q}) [S_{\lambda\lambda}(\mathbf{q}) S_{\lambda'\lambda'}(\mathbf{q})]^{-1/2}$ has been chosen. Varying the aspect ratio $X_0 = \frac{a}{b}$ and the volume fraction $\varphi = \frac{\pi}{6} ab^2$, we have located the glass transition line, at which for l, l' both even a nontrivial solution for $F_{\lambda\lambda'}(\mathbf{q})$ bifurcates.

This has been done by approaching the glass transition point from the glass side. Fig. 1 shows an example where $F_{21,21}(\mathbf{q} = \mathbf{0})$ is represented as function of a for fixed b . The fit with a square root, predicted by MCT for a

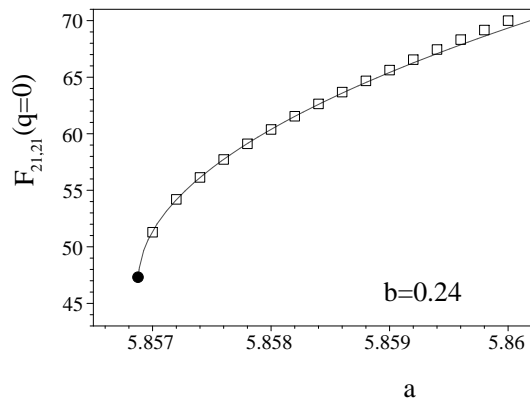


FIG. 1: a -dependence of the NEP $F_{21,21}(\mathbf{q} = \mathbf{0})$ in the vicinity of the glass transition point for fixed $b = 0.24$ and different values of a (squares). Also shown is the square root fit $47 + 400\sqrt{a - 5.85688}$, leading to the critical values $(a_c, F_{21,21}^c(\mathbf{0}))$ (black dot). Note the rather large prefactor of the square root.

type B-transition [5] allows to locate the glass transition point $a_c(b)$ for fixed $b = 0.24$ up to a relative deviation better than 10^{-4} ! The NEP $F_{21,21}(\mathbf{0})$ for $a = 5.857$ (see Fig. 10) deviates less than ten percent from the critical NEP $F_{21,21}^c(\mathbf{0}) = 47$ at $a_c = 5.85688$, and no qualitative change is to be expected on further approach towards a_c .

A. Phase diagram

The glass transition line $\varphi_c(X_0)$ obtained in this way is shown in Fig. 2. Fig. 2 also contains the equilibrium phase transition line $\varphi_{\text{eq}}(X_0)$ from MC-simulations, and the line $\varphi_{\text{PY}}(X_0)$. Also shown is the curve $\varphi_{\text{extra}}(X_0)$ where the extrapolated OZ/PY static orientational correlators for $X_0 \gtrsim 4$ at the zone center diverge. $\varphi_{\text{eq}}(X_0)$ and $\varphi_{\text{PY}}(X_0)$ were obtained from the corresponding lines $a_{\text{eq}}(b)$ and $a_{\text{PY}}(b)$ of Ref. [33]. Finally, the solid line with the cusp at $X_0 = 1$ is the location of all $\varphi(X_0)$ at which the rotators start to interact.

At $\varphi_{\text{eq}}(X_0)$, an equilibrium phase transition from a (dynamically) disordered to an orientationally ordered phase occurs. The line $\varphi_{\text{PY}}(X_0)$ locates the (X_0, φ) -pairs for which the iterative numerical procedure to solve the OZ/PY equations becomes unstable. This is associated with some of the maxima of $\mathbf{S}(\mathbf{q})$ becoming very large, giving evidence of a divergency. Since the X_0 -dependence of φ_{eq} and φ_{PY} is qualitatively similar, this behavior may indicate an equilibrium phase transition, as speculated for a liquid of hard ellipsoids [41]. However, in contrast to the latter, the deviation of $\varphi_{\text{PY}}(X_0)$ from $\varphi_{\text{eq}}(X_0)$ is much larger, especially for prolate ellipsoids. Using the static correlators from OZ/PY-theory as an input for the calculation of the NEP from Eqs. (22) and (23) we have found a glass transition for $X_0 \lesssim 0.7$ and $2 \lesssim X_0 \lesssim 2.5$, only. For $0.7 \lesssim X_0 \lesssim 2$ and $X_0 \gtrsim 4$ the system is ergodic for all $\varphi \leq \varphi_{\text{PY}}(X_0)$, because the static correlators at

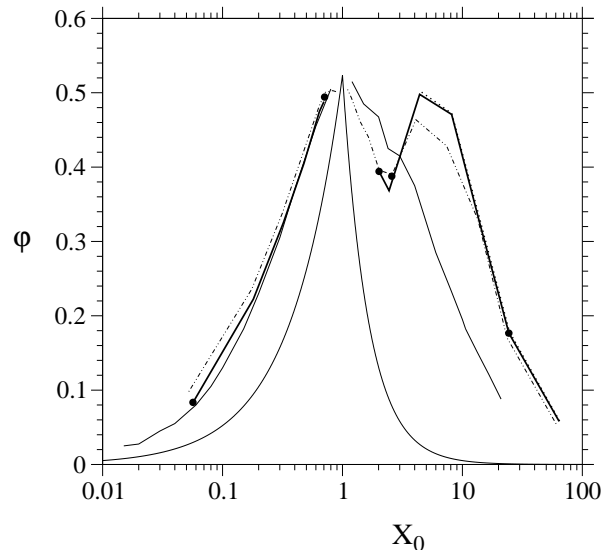


FIG. 2: Phase diagram of hard ellipsoids on a sc lattice. Shown is the curve below which the ellipsoids are free rotators (full line with cusp at $X_0 = 1$), the equilibrium phase transition line $\varphi_{\text{eq}}(X_0)$ from MC simulations (full thin lines), the line $\varphi_{\text{PY}}(X_0)$ of highest densities to be reached by numerical solution of the OZ/PY equations (dash-dotted lines), the line $\varphi_{\text{extra}}(X_0)$ for $X_0 \gtrsim 4$, where the extrapolated OZ/PY results diverge (dotted line) and the MCT glass transition line $\varphi_c(X_0)$ (full thick lines). For $X_0 \gtrsim 8$, $\varphi_{\text{extra}}(X_0)$ and $\varphi_c(X_0)$ are almost identical. • denote the five state points for which the nonergodicity parameters presented in Figs. 3-12 were calculated.

the Brillouin zone center and/or edge are too small. Unfortunately, the iterative procedure to solve the OZ/PY equations for $0.7 \lesssim X_0 \lesssim 2$ and $X_0 \gtrsim 4$ becomes unstable for $\varphi \geq \varphi_{\text{PY}}(X_0)$. Therefore, we have decided to extrapolate the static correlators to $\varphi \geq \varphi_{\text{PY}}(X_0)$. This extrapolation is guided by the physical assumption that long range orientational order should occur at the line $\varphi_{\text{extra}}(X_0)$. It only works for $X_0 \gtrsim 4$, but not for the gap in between $X_0 \approx 0.7$ and $X_0 \approx 2$. Accordingly, the missing glass transition line for $0.7 \lesssim X_0 \lesssim 2$ first of all is based upon the lack of the static input. Since the ergodic and nonergodic phase are separated by a critical line of Type-B transitions [5, 6], $\varphi_c(X_0)$ can not terminate at $X_0 \approx 0.7$ or $X_0 \approx 2$. There exist two possible scenarios for $\varphi_c(X_0)$ within this gap. First, $\varphi_c(X_0)$ converges to $\varphi_c(X_0 = 1)$ from above and below $X_0 = 1$, with a possible cusp at $X_0 = 1$. Second, $\varphi_c(X_0) \rightarrow \varphi_{\text{max}}(X_0^\pm)$ for $X_0 \rightarrow X_0^\pm$ with $0.7 \lesssim X_0^- < 1$ and $1 < X_0^+ \lesssim 2$, where $\varphi_{\text{max}}(X_0)$ is the maximum possible volume fraction of an orientationally disordered configuration for given X_0 . The second scenario would imply that there is no glass transition for $X_0^- \leq X_0 \leq X_0^+$, i.e. for ellipsoids which are not sufficiently aspherical.

The non-monotonous behavior of $\varphi_{\text{PY}}(X_0)$ for prolate ellipsoids with $1 < X_0 \lesssim 4$, which induces a non-monotonicity of $\varphi_c(X_0)$, seems to be an artefact of the

PY approximation, as our MC results for hard prolate ellipsoids suggest, though the static orientational correlators from OZ/PY theory are *qualitatively* correct, anyway [33].

If it is true that the divergence of the PY solutions corresponds to an equilibrium phase transition, this implies that the ideal glass transition is driven by the growth of some $S_{\lambda\lambda'}(\mathbf{q})$ at the zone center or/and edge due to the growth of the orientational order, as will be seen in the following figures. This is quite similar to the central peak phenomenon above the equilibrium transition temperature at structural phase transitions of first and second order [42]. The central peak can be interpreted as a quasi-nonergodic behavior and has also been described by MCT [43].

The freezing of the l, l' odd correlators occurs beyond the l, l' even glass transition line and is treated in subsection III D.

B. Critical nonergodicity parameters

The critical NEP $F_{\lambda\lambda'}^c(\mathbf{q})$ and the normalized critical NEP $f_{\lambda\lambda'}^c(\mathbf{q})$ together with the static orientational correlators are shown in Figs. 3, 6, 7, 9 and 10 for oblate and prolate ellipsoids, respectively, along the three highly symmetric directions in reciprocal space from the zone center to its edge. For each of the three directions and each matrix element, a separate subfigure is provided, where the indices $lml'm'$ are displayed at the top of each figure. We have restricted our illustrations to the diagonal elements $l = l' = 2, m = m' = 0, 1, 2$ and $l = l' = 4, m = m' = 0, 1, 2, 3, 4$, and the off-diagonal elements $l = 2, l' = 4, m = m' = 0, 1, 2$. By the symmetries of the cubic lattice, these correlators are all real. The scales on the l.h.s. of each tableau belong to $S_{\lambda\lambda'}(\mathbf{q})$ and $F_{\lambda\lambda'}^c(\mathbf{q})$, those on the r.h.s. to $f_{\lambda\lambda'}^c(\mathbf{q})$. Note the different scales of the axes for different values of $m = m'$.

For two pairs (a, b) we also present the corresponding tensorial quantities in real space. Figs. 4 and 8 show log-lin representations of the direct space static orientational correlators $G_{xyz, \lambda\lambda'}$ and the corresponding NEP $F_{xyz, \lambda\lambda'}^c = \lim_{t \rightarrow \infty} G_{xyz, \lambda\lambda'}(t)$ along lattice directions of high symmetry, i.e. $xyz = 00n, 0nn$ and nnn for $n = 0, 1, \dots, 8$. Along these directions, all $G_{xyz, \lambda\lambda'}$ and $F_{xyz, \lambda\lambda'}^c$ are real, too, for $\lambda\lambda'$ as above. Note that a step $\Delta n = 1$ corresponds to different lengths in direct space, namely 1, $\sqrt{2}$ and $\sqrt{3}$ for the different lattice directions. For each $m = m'$ and each lattice direction, a separate figure is provided and a logarithmic plotting has been chosen for positive and negative values of $G_{xyz, \lambda\lambda'}$ and $F_{xyz, \lambda\lambda'}^c$ separately, i.e. the negative values are presented as $-\ln |G_{xyz, \lambda\lambda'}|$ and $-\ln |F_{xyz, \lambda\lambda'}^c|$, respectively. The values of $xyz, lml'm'$ are included in each subfigure.

Figs. 3-6 present the NEP for $l = l' = 2$ and $l' = 2, 4$ for oblate ellipsoids with $a = 0.08$ and $b = 1.412$, which yields $(X_0, \varphi) \cong (0.0567, 0.0835)$. In comparison to liquids, the NEP possess less structure in q -space. For

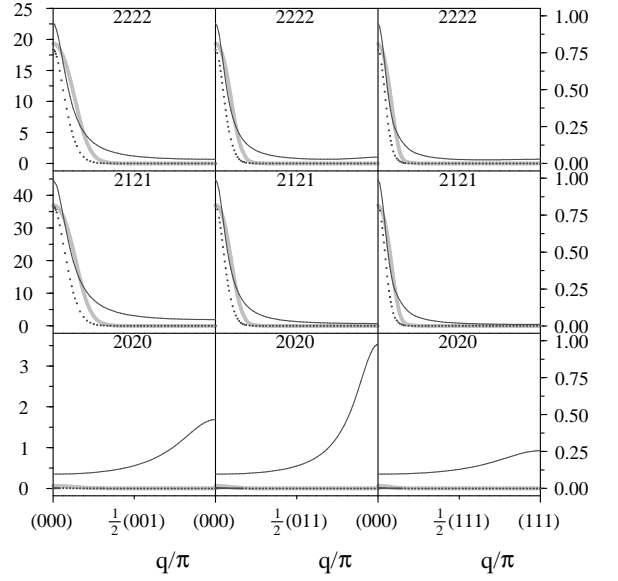


FIG. 3: \mathbf{q} -dependence of the nonergodicity parameters $F_{\lambda\lambda'}^c(\mathbf{q})$ (dotted lines), the normalized ones $f_{\lambda\lambda'}^c(\mathbf{q}) = F_{\lambda\lambda'}^c(\mathbf{q}) [S_{\lambda\lambda}(\mathbf{q}) S_{\lambda'\lambda'}(\mathbf{q})]^{-1/2}$ (thick grey lines) and of the static structure factors $S_{\lambda\lambda'}(\mathbf{q})$ (solid lines) for $l = l' = 2$ and $m = m' = 0, 1, 2$. Results are shown within the first Brillouin zone along the three highly symmetric reciprocal space directions for *oblate* ellipsoids with $a = 0.08$ and $b = 1.412$, i.e. $(X_0, \varphi) \cong (0.0567, 0.0835)$.

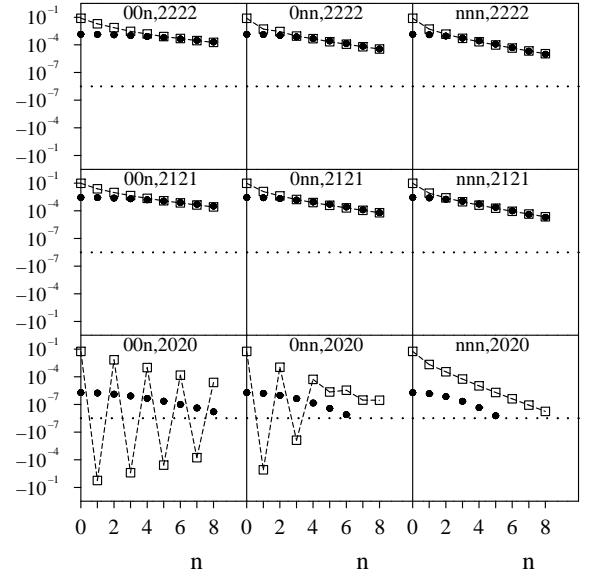


FIG. 4: The nonergodicity parameters $F_{xyz, \lambda\lambda'}^c$ in real space (solid circles) and the static orientational density correlators $G_{xyz, \lambda\lambda'}$ (squares; dashed lines are a guide to the eye) along the three highly symmetric direct lattice directions for *oblate* ellipsoids with $a = 0.08$ and $b = 1.412$, i.e. $(X_0, \varphi) \cong (0.0567, 0.0835)$. Shown are the diagonal correlators for $l = l' = 2, m = m' = 0, 1, 2$ and $xyz = 00n, 0nn$ or nnn for $n = 0, 1, \dots, 8$.

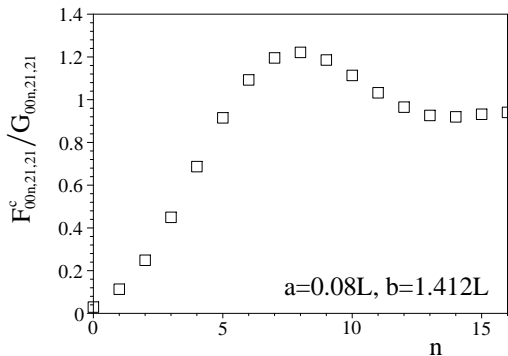


FIG. 5: n -dependence of the ratio $F_{00n,21,21}^c/G_{00n,21,21}$ of the NEP $F_{00n,21,21}^c$ and his static counterpart $G_{00n,21,21}$ for *oblate* ellipsoids with $a = 0.08$ and $b = 1.412$, i.e. $(X_0, \varphi) \cong (0.0567, 0.0835)$.

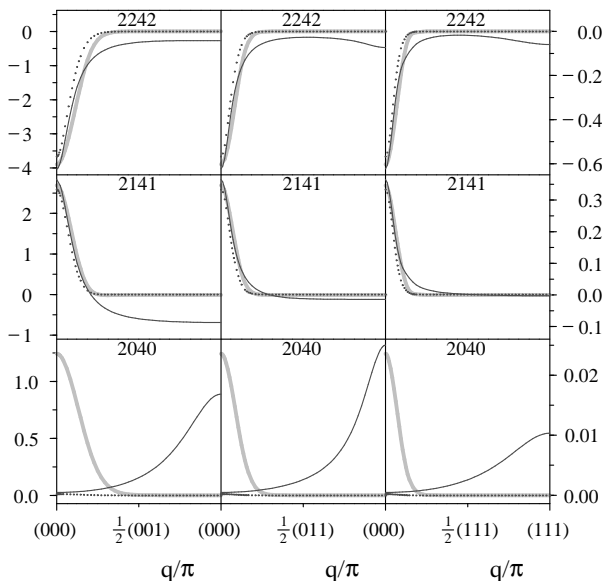


FIG. 6: Same as Fig. 3, but for $l = 2, l' = 4$.

$l = l' = 2$, they are maximum exclusively at the zone *center*. A similar behavior is found for $l \neq l'$ (cf. Fig. 6), but here, e.g. for $m = m' = 2$, minima appear instead of maxima. None of the maxima of the static structure factors $S_{2m,2m}(\mathbf{q})$ and maxima/minima of $S_{2m,4m}(\mathbf{q})$ at the zone *boundary* persists in the limit $t \rightarrow \infty$. Since these maxima belong to alternating orientational density fluctuations, this proves that such alternating local arrangements of the particles do not arrest. This can also be seen in real space. Fig. 4 exhibits the static orientational density correlators $G_{xyz,2m,2m}$ and the $F_{xyz,2m,2m}^c$ for $a = 0.08$ and $b = 1.412$. Indeed, the oscillations in the correlators $G_{00n,20,20}$ and $G_{0nn,20,20}$ vanish completely in the long time limit, while the monotonous decay with n of the ($m = m' > 0$)-quantities is rather stable, even for infinite time. The almost vanishing of some critical NEP, however, does not require oscillations in the cor-

responding $G_{xyz,\lambda\lambda'}$, as can be seen from $G_{nnn,20,20}$ and $F_{nnn,20,20}^c$. Another remarkable feature is the behavior at small n , particularly at $n = 0$. Fig. 4 demonstrates that, e.g., the magnitude of $F_{000,2m,2m}^c$ for $m = 1, 2$ is only a few percent or even less of that of $G_{000,2m,2m}$. Fig. 5 shows that the ratio $F_{00n,21,21}^c/G_{00n,21,21}$ becomes very small as n is lowered. A similar behavior has been found for all values (X_0, φ) on the glass transition lines we have investigated. The dips in $F_{xyz,\lambda\lambda'}^c/G_{xyz,\lambda\lambda'}$ at $n = 0$ demonstrate that the relaxation of the “self” part of the orientational correlators is practically not arrested by an orientational cage.

Moving for oblate ellipsoids along the glass transition line towards the spherical limit $X_0 = 1$, no qualitatively new behavior of the critical NEP is found, but it resembles always the characteristics of Figs. 3 and 6. However, this picture will change as we turn for oblate ellipsoids into the glass phase, as will be seen in subsection III C.

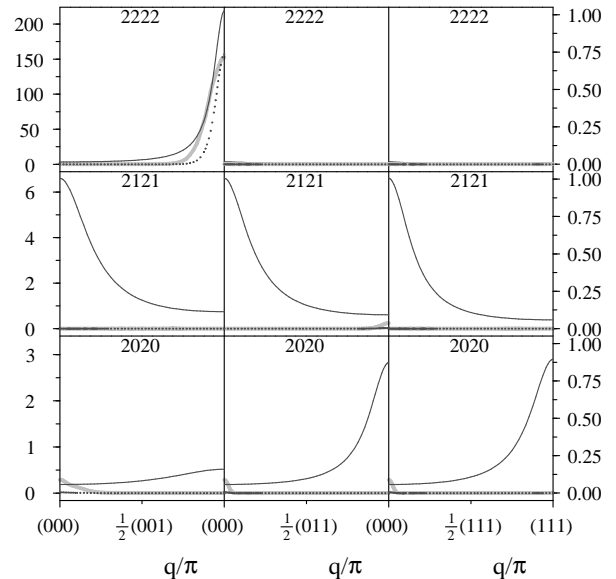


FIG. 7: Same as Fig. 3, but for *prolate* ellipsoids with $a = 1.4524$ and $b = 0.72$, i.e. $(X_0, \varphi) \cong (2.02, 0.394)$.

The q -dependence of the critical NEP for *prolate* ellipsoids is sensitive on the shape of the ellipsoids (see Figs. 7, 9 and 10). The reader should note the higher values of the maxima in $S_{\lambda\lambda'}(\mathbf{q})$, which are necessary to get a glass transition, compared to the corresponding correlators for oblate ellipsoids. Let us have a closer look at prolate ellipsoids with $a = 1.4524$ and $b = 0.72$, i.e. $(X_0, \varphi) \cong (2.02, 0.394)$. Fig. 7 shows that the structural arrest of these ellipsoids is completely different from that of oblate ones. The huge peak in $F_{22,22}^c(\mathbf{q} = (0, 0, \pi))$ at the zone boundary has a height of 157 and dominates the transition. Since this peak belongs to a wavelength of period two, it leads to strong frozen oscillations in the orientational density fluctuations on the lattice, as can be seen in direct space from Fig. 8. Note that for the correlators $F_{00n,21,21}^c$ almost no decay exists if n is increased. Again, like for oblate ellipsoids, the frozen $F_{xyz,20,20}^c$ seem

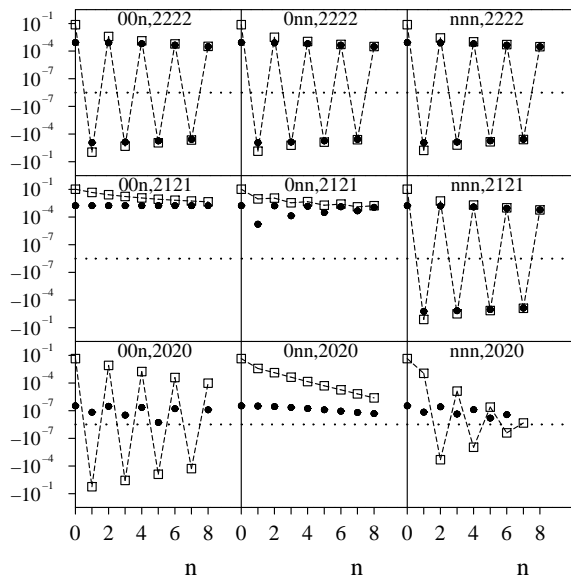


FIG. 8: Same as Fig. 4, but for *prolate* ellipsoids with $a = 1.4524$ and $b = 0.72$, i.e. $(X_0, \varphi) \cong (2.02, 0.394)$.

to play a special role, since they are much weaker than the NEP for $m = m' > 0$. Fig. 9 shows the diagonal correlators for $l = l' = 4$. Note the very small scale for the static structure factors and NEP, in comparison with Fig. 7. Fig. 9 shows other interesting features of the MCT results for molecular crystals: besides the appearance of simultaneous maxima of the normalized NEP at the zone center and its boundary (see $f_{42,42}(\mathbf{q})$ along the fourfold reciprocal space direction), the rule that the normalized NEP in reciprocal space are in phase with the corresponding static correlators [44] is violated.

Finally, it must be said that the static structure factors for ellipsoids with $a = 1.4524$, $b = 0.72$ have been calculated by OZ/PY theory. But MC results [33] for other values of (a, b) in the vicinity of these parameters show that OZ/PY overestimates the maxima at the zone boundary in this region of the phase diagram. Therefore, the interpretation of Figs. 7-9 should be taken with some caution. Perhaps this overestimation is the indirect cause for the dip in $\varphi_{PY}(X_0)$ for $2 \lesssim X \lesssim 4$ (see Fig. 2). Why OZ/PY fails in this region of ellipsoids is currently unknown.

As we turn to very elongated prolate ellipsoids, the transition scenario becomes simpler again. Fig. 10 for $a = 5.857$ and $b = 0.24$ [yielding $(X_0, \varphi) \cong (24.4, 0.177)$] serve as an illustration. The behavior of the ($l = l' = 2$)-NEP with peaks at the zone center reminds one of the NEP for flat oblate ellipsoids (see Fig. 3). This means that for long prolate ellipsoids only nematic-like orientational fluctuations may freeze. Such an extreme narrowness of the peaks at $\mathbf{q} = \mathbf{0}$ as seen in Fig. 10 is observed for prolate ellipsoids with $X_0 \gtrsim 8$ only, indicating the huge spatial extension of the frozen nematic-like fluctuations.

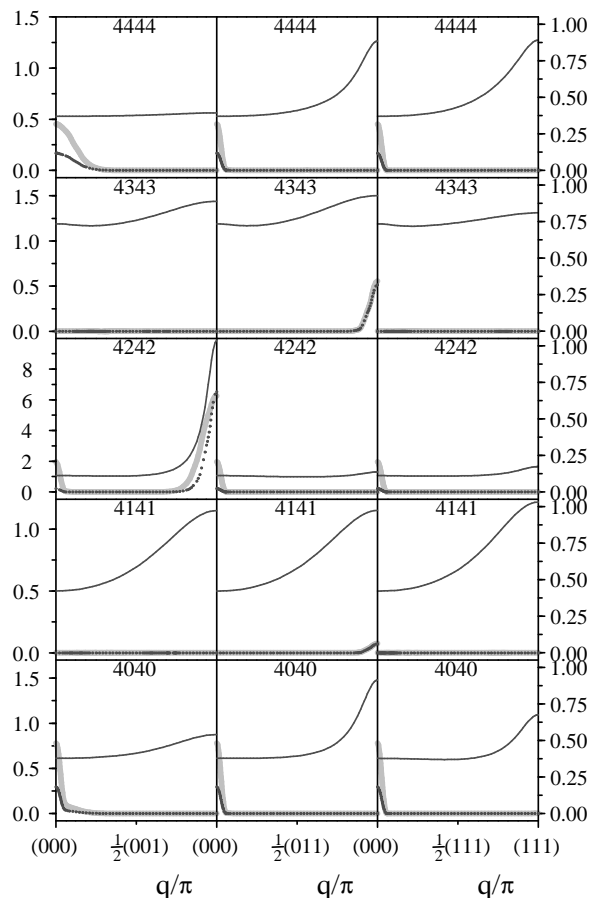


FIG. 9: Same as Fig. 3, but for *prolate* ellipsoids with $a = 1.4524$ and $b = 0.72$, i.e. $(X_0, \varphi) \cong (2.02, 0.394)$, and for $l = l' = 4$, $m = m' = 0, 1, 2, 3, 4$.

C. Nonergodicity parameters in the glass phase

In this subsection, we show by means of two examples how the NEP change in comparison to the critical NEP on moving slightly into the glass phase. The corresponding pairs (X_0, φ) are indicated in Fig. 2, too.

For densely packed oblate ellipsoids with $a = 0.78$ and $b = 1.1$, i.e. $(X_0, \varphi) \cong (0.709, 0.494)$ in the glass phase, the prototypical behavior of the critical NEP for oblate ellipsoids on the glass transition line shown in Figs. 3 and 6 is clearly changed, as can be seen from Fig. 11 [53]. Now, the Gaussian-like shape of the normalized NEP is much broader, indicating an enhanced arrest of orientational density fluctuations for $\mathbf{q} \neq \mathbf{0}$, which is expected due to the high packing fraction. This leads to a deviation of the frozen orientational correlators in direct space from the exclusive monotonous decay, which is present almost everywhere along the glass transition line for oblate ellipsoids. For example, the frozen $F_{00n,20,20}$ for the (a, b) -pair of Fig. 11 (not shown here) have weak oscillations, reminiscent of the strong oscillations being present in the associated static $G_{00n,20,20}$.

Considering prolate ellipsoids with $a = 1.7$ and $b =$

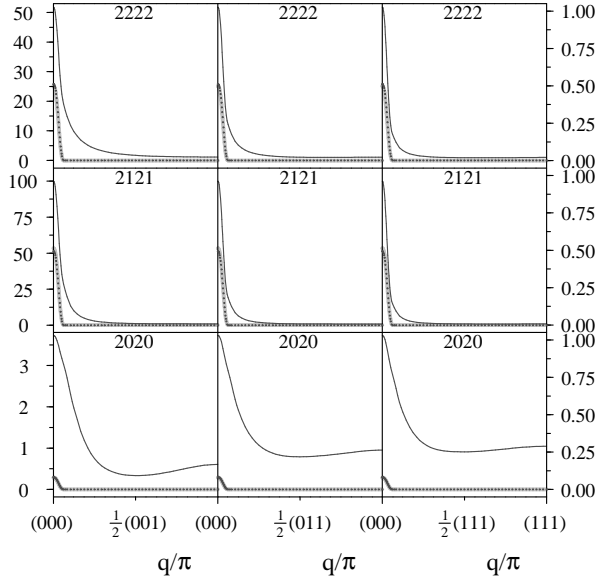


FIG. 10: Same as Fig. 3, but for *prolate* ellipsoids with $a = 5.857$ and $b = 0.24$, i.e. $(X_0, \varphi) \cong (24.4, 0.177)$.

0.66, i.e. $(X_0, \varphi) \cong (2.58, 0.389)$, slightly above the glass transition line, many different patterns of behavior occur in the NEP, as can be seen from Fig. 12. This figure can directly be compared with Fig. 7, since the ellipsoids for both figures have almost the same packing fraction. Again, for one and the same NEP there partly exist simultaneous maxima at the zone center and its boundary. Accordingly, in the limit of long times, we have frozen density-density correlators with either oscillatory or monotonous behavior, depending on $\lambda\lambda'$.

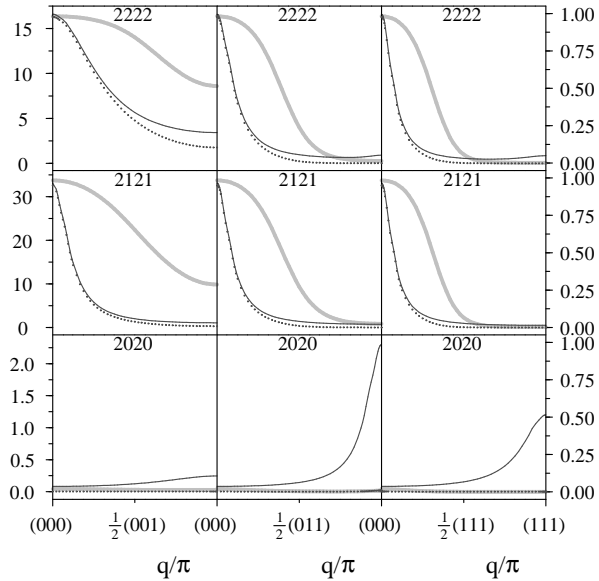


FIG. 11: Same as Fig. 3, but for *oblate* ellipsoids with $a = 0.78$ and $b = 1.1$, i.e. $(X_0, \varphi) \cong (0.709, 0.494)$, above the glass line.

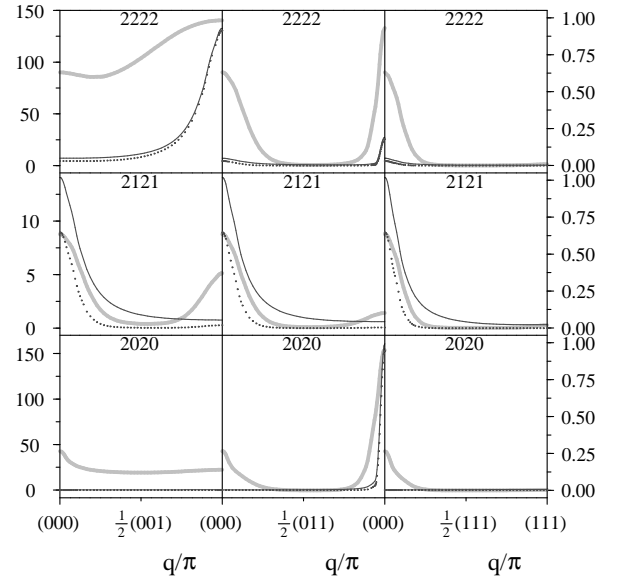


FIG. 12: Same as Fig. 3, but for *prolate* ellipsoids with $a = 1.7$ and $b = 0.66$, i.e. $(X_0, \varphi) \cong (2.58, 0.389)$, above the glass line.

D. Glass transition of the l, l' odd correlators

So far we have discussed the NEP for l, l' even. For l, l' odd only the “self” part of the NEP is nonzero. It is useful to investigate the normalized, rotationally invariant “self” part of the NEP, i.e.

$$f_l^{(s)} = \frac{\sum_{m=-l}^l F_{000,lm,lm}}{\sum_{m=-l}^l G_{000,lm,lm}}. \quad (26)$$

Values for $f_l^{(s)}$ are given in Table I for those pairs (a, b) for which the glass transition has been found for l, l' odd. For comparison, the $f_l^{(s)}$ for l even are given in Table I, too. The relation

$$f_l^{(s)} < f_{l'}^{(s)}, \quad l > l', \quad (27)$$

which is similar to

$$f^c(q) < f^c(q'), \quad q > q' \quad (28)$$

for simple liquids, seems to be fulfilled for even and odd l separately. Note that the pairs (a, b) in Table I are located in the glass phase for l, l' even.

(a, b)	$l = 1$	$l = 2$	$l = 3$	$l = 4$
(0.776, 1.1)	0.203	0.208	0.124	0.106
(0.778, 1.1)	0.406	0.268	0.262	0.143
(0.78, 1.1)	0.546	0.333	0.371	0.185
(1.7, 0.66)	3.00×10^{-2}	0.197	8.14×10^{-3}	3.93×10^{-2}

TABLE I: Selected normalized NEP $f_l^{(s)}$ of the “self” part of the orientational density-density correlation function (see Eqs. (24), (25)).

IV. DISCUSSION AND CONCLUSIONS

We have extended the mode coupling theory (MCT) for liquids to molecular crystals. The natural choice is the use of tensorial correlators, instead of correlators defined in a site-site representation [45]. This leads for the dynamical correlators $S_{\lambda\lambda'}(\mathbf{q}, t)$ to an integro-differential equation of second order in time. Truncating l at l_{\max} , this set of equations is equivalent to the corresponding equation for a multi-component liquid of isotropic particles (for binary systems see, e.g., [46]). The memory kernel is approximated in the framework of MCT. The main differences to liquids are (i) the occurrence of Umklapp processes, if the sum of the wave vectors \mathbf{q}_1 , \mathbf{q}_2 of the orientational density modes $\delta\rho_{\lambda_1}(\mathbf{q}_1)$ and $\delta\rho_{\lambda_2}(\mathbf{q}_2)$ is outside of the first Brillouin zone, (ii) besides the static two-point orientational correlators $S_{\lambda\lambda'}(\mathbf{q})$ the need of the one-molecule orientational density $\rho^{(1)}(\Omega)$ as an input for the vertices of the memory kernel and (iii) the anisotropy of the static orientational current density correlators $J_{\lambda\lambda'}$ which do not cancel completely from the memory kernel $m_{\lambda\lambda'}(\mathbf{q}, t)$. Nevertheless, the factor $k_B T/I$ of $J_{\lambda\lambda'}$ drops out. Accordingly, the glassy dynamics and the ideal glass transition does not exhibit inertia effects, i.e. they are independent on I , the moment of inertia. Additionally, for rigid lattices, all $l, l' = 0$ tensorial correlators vanish and can be skipped, due to the lack of TDOF.

In order to discuss this set of MCT-equations for molecular crystals we have chosen hard ellipsoids of revolution with aspect ratio $X_0 = a/b$ fixed with their centers of mass at the sites of a sc-lattice with lattice constant equal to one. Increasing the size of the ellipsoids, which is equivalent to a decrease of the lattice constant, results in an increase of steric hindrance and finally in an orientational glass transition at the MCT-glass transition line $\varphi_c(X_0)$ shown in Fig. 2 for oblate and prolate ellipsoids. Since this orientational glass transition is mainly driven by the growth of $S_{\lambda\lambda'}(\mathbf{q})$ at the zone center or/and the zone edge, its origin lies in the growth of the orientational order close to but below the equilibrium phase transition line from OZ/PY theory. This is quite similar to what has been found for a liquid of hard ellipsoids [39] if the aspect ratio becomes larger than about 2 or smaller than about $\frac{1}{2}$. However, there is a difference between the molecular liquid (of ellipsoids) and the molecular crystal. Whereas the former already undergoes a glass transition for $X_0 > 2$ or $X_0 < \frac{1}{2}$ when $S_{2m,2m}(\mathbf{0})$ is of order one, it must be $S_{2m,2m}(\mathbf{0})$ of order 10 for oblate (cf. Fig. 3) or even order 100 for prolate ellipsoids (cf. Fig. 7). This proves that the translational degrees of freedom of the liquid still have a strong influence on the glass formation, although they are not primarily responsible for the transition for $X_0 > 2$ and $X_0 < \frac{1}{2}$. This finding is consistent with results found from a MD simulation for difluorotetrachloroethane in its supercooled liquid and plastic crystal phase [47]. For both phases, the glass transition temperatures T_c^{liquid} and $T_c^{\text{plastic crystal}}$ were determined. That $T_c^{\text{liquid}} \cong 139\text{K} > T_c^{\text{plastic crystal}} \cong 129\text{K}$ implies

that the translational degrees of freedom of a liquid enhance the glass formation which might be related to a facilitated cage formation for systems where the center of mass of the particles can move freely.

Comparing $S_{\lambda\lambda'}(\mathbf{q})$ on the glass transition line for oblate (Figs. 3 and 6) with prolate ellipsoids (Figs. 7 and 9-10) already shows that the tendency to an orientational glass formation for oblate ellipsoids is larger than for prolate ones. This can also be seen from Fig. 2 since the distance $\varphi_{\text{PY}}(X_0) - \varphi_c(X_0)$ is large for very flat oblate ellipsoids, only. This difference may be explained as follows. If we fix the length a of prolate ellipsoids and decrease their thickness b to zero, then the excluded volume interaction becomes zero. Particularly, the static correlators become trivial, which leads to vanishing vertices and consequently to a disappearance of the MCT glass transition. If on the other hand we fix the diameter b of the oblate ellipsoids and decrease their thickness a to zero the excluded volume interaction still exists for $a = 0$. This seems to be an important difference between oblate and prolate particles.

From the solution of the MCT equations for $t \rightarrow \infty$ we obtained results for the critical NEP $F_{\lambda\lambda'}^c(\mathbf{q})$ and the corresponding normalized ones, $f_{\lambda\lambda'}^c(\mathbf{q})$, as well as NEP deeper in the glass. Due to the lattice translational invariance, \mathbf{q} can be restricted to the first Brillouin zone. Within this zone the critical NEP do not have much structure. Almost all of them either exhibit a maximum (or minimum for $l \neq l'$) at the zone center and/or at its edge, depending on $\lambda\lambda'$ and the direction of \mathbf{q} . However, going deeper into the glass and varying the ellipsoid shape, i.e. X_0 and/or φ , leads to significant changes in the \mathbf{q} -dependence especially of the normalized NEP, as demonstrated in Figs. 11 and 12.

The MD-simulations for cyanoadamantane [16] and chloradamantane [18] reveal quite similar glassy dynamics as found for supercooled liquids [7, 8, 9]. Particularly, the authors of Refs. [16, 18] stress that their molecular crystals can be supercooled and that the relaxational dynamics is consistent with MCT predictions, at least where this has been checked [16, 18]. Since both model systems exhibit tremendous slowing down in the supercooled regime an orientational glass transition or at least a crossover from ergodic to quasi-nonergodic dynamics must also occur in the supercooled phase. This is different from what we have found for the hard ellipsoids. In our case the glass transition line is located within the dynamically disordered equilibrium phase of PY theory, which itself is a consequence of the static input taken from PY theory. It would be very interesting to insert the static correlators [54] from the MD simulations in the supercooled phase into our MCT equations and to check whether one obtains a glass transition. The investigation of hard ellipsoids on the sc lattice has demonstrated that the magnitude of the extrema in $S_{\lambda\lambda'}(\mathbf{q})$ at the zone center or/and edge must be rather large (at least for prolate particles). It is not obvious that the simulational results in the supercooled phase fulfill this criterion. Of course,

it could be that the *average* height of $S_{\lambda\lambda'}(\mathbf{q})$ in q -space is much larger than for the ellipsoids such that large maxima/minima of $S_{\lambda\lambda'}(\mathbf{q})$ at the zone center and/or edge are not really necessary. We hope that these questions can be answered in future.

To conclude, we have shown that MCT can be derived for molecular crystals, as well. Whether or not the MCT approximation (which mainly consists of the factorization of a time dependent four point correlator) is also a reasonable approximation for molecular crystals as it is for glass-forming liquids has to be investigated by comparison of the results from present MCT for molecular crystals with simulational and experimental results. As already mentioned above our conventional MCT approach will become worse if the thickness of *prolate* particles becomes small. In that case it is the entanglement which is responsible for glassy dynamics [22, 23]. This requires a different theoretical description, as recently discussed [48, 49].

APPENDIX A: CALCULATION OF $J_{\lambda\lambda'}(\mathbf{q}) \equiv J_{\lambda\lambda'}$

Substituting the λ -Fourier transform $j_\lambda(\mathbf{q})$ of $j_n(\Omega)$ (Eq. (6)) into Eq. (11) yields

$$J_{\lambda\lambda'}(\mathbf{q}) = \frac{4\pi}{N} i^{l'-l} \sum_{nn'} e^{i\mathbf{q}\cdot\mathbf{x}_{nn'}} \times \langle (\boldsymbol{\omega}_n \cdot \hat{\mathbf{L}}_{\Omega_n} Y_\lambda(\Omega_n))^* (\boldsymbol{\omega}_{n'} \cdot \hat{\mathbf{L}}_{\Omega_{n'}} Y_{\lambda'}(\Omega_{n'})) \rangle. \quad (\text{A1})$$

Since $\boldsymbol{\omega}_n \cdot \hat{\mathbf{L}}_{\Omega_n} = \boldsymbol{\omega}'_n \cdot \hat{\mathbf{L}}'_{\Omega_n}$ (where the primed quantities refer to the body fixed frame) we get for the canonical average in Eq. (A1) in close analogy to molecular liquids [28]

$$\begin{aligned} \langle \dots \rangle &= \sum_{\alpha\alpha'} \langle \omega_n'^\alpha \omega_{n'}'^{\alpha'} \rangle \langle (\hat{L}'_{\Omega_n} Y_\lambda(\Omega_n))^* (\hat{L}'_{\Omega_{n'}} Y_{\lambda'}(\Omega_{n'})) \rangle \\ &= \sum_{\alpha\alpha'} \frac{kT}{I} \delta_{nn'} \delta_{\alpha\alpha'} \langle (\hat{L}'_{\Omega_n} Y_\lambda(\Omega_n))^* (\hat{L}'_{\Omega_{n'}} Y_{\lambda'}(\Omega_{n'})) \rangle, \end{aligned} \quad (\text{A2})$$

where, $\alpha = x, y, z$ are the cartesian components in the body fixed frame. This leads to

$$J_{\lambda\lambda'}(\mathbf{q}) = 4\pi \frac{kT}{I} i^{l'-l} \langle (\hat{\mathbf{L}}_{\Omega_n} Y_\lambda(\Omega_n))^* \cdot (\hat{\mathbf{L}}_{\Omega_{n'}} Y_{\lambda'}(\Omega_{n'})) \rangle, \quad (\text{A3})$$

which is \mathbf{q} - and n -independent, and can therefore be evaluated for arbitrary n .

Using $\hat{L}_\Omega^\alpha Y_{lm}(\Omega) = \sum_{m'=-l}^l L_{l,mm'}^\alpha Y_{lm'}(\Omega)$ and the product rule for the spherical harmonics and substituting the explicit expression for $L_{l,mm'}^\alpha$ we get with $c(l, l', l'')$ as in (C4)

$$\begin{aligned} J_{\lambda\lambda'}(\mathbf{q}) &= 4\pi \frac{kT}{I} i^{l'-l} (-1)^m \sum_{\lambda''} \left[mm' C(ll'l'', -mm'm'') \right. \\ &\quad - \frac{1}{2} \sqrt{l(l+1) - m(m+1)} \sqrt{l'(l'+1) - m'(m'+1)} C(ll'l'', -m-1, m'+1, m'') \\ &\quad \left. - \frac{1}{2} \sqrt{l(l+1) - m(m-1)} \sqrt{l'(l'+1) - m'(m'-1)} C(ll'l'', -m+1, m'-1, m'') \right] c(ll'l'') \langle Y_{\lambda''} \rangle. \end{aligned} \quad (\text{A4})$$

This expression strongly simplifies since

$$[\dots] c(ll'l'') = -\frac{1}{2} \sqrt{l(l+1)} \sqrt{l'(l'+1)} \left[\frac{(2l+1)(2l'+1)}{4\pi(2l''+1)} \right]^{\frac{1}{2}} \{C(ll'l'', 1-10) + C(ll'l'', -110)\} C(ll'l'', -mm'm''). \quad (\text{A5})$$

This leads to the final result

$$\begin{aligned} J_{\lambda\lambda'}(\mathbf{q}) &= 4\pi \frac{kT}{I} i^{l'-l} (-1)^{m+1} \frac{1}{2} \sqrt{l(l+1)} \sqrt{l'(l'+1)} \times \\ &\quad \times \sum_{\lambda''} \left[\frac{(2l+1)(2l'+1)}{4\pi(2l''+1)} \right]^{\frac{1}{2}} \{C(ll'l'', 1-10) + C(ll'l'', -110)\} C(ll'l'', -mm'm'') \langle Y_{\lambda''} \rangle. \end{aligned} \quad (\text{A6})$$

Note that $\langle Y_\lambda \rangle$ is given by

$$\langle Y_\lambda \rangle = \int d\Omega \rho^{(1)}(\Omega) Y_\lambda(\Omega) = (-i)^l \rho_\lambda^{(1)}, \quad (\text{A7})$$

i.e. $J_{\lambda\lambda'}(\mathbf{q}) \equiv J_{\lambda\lambda'}$ only involves the λ -transform of $\rho^{(1)}(\Omega)$.

APPENDIX B: MODE COUPLING APPROXIMATION

In this appendix we shortly describe the mode coupling approximation leading to the results presented by Eqs. (15)-(19).

The derivation of the Mori-Zwanzig equation is standard by using the projectors onto the slow variables $\delta\rho_\lambda(\mathbf{q})$ and $j_\lambda(\mathbf{q})$,

$$P_\rho = \frac{4\pi}{N} \sum'_{\lambda\lambda'} |\delta\rho_\lambda(\mathbf{q})\rangle (\mathbf{S}^{-1}(\mathbf{q}))_{\lambda\lambda'} \langle \delta\rho_{\lambda'}^*(\mathbf{q}) |, \quad (\text{B1})$$

$$P_j = \frac{4\pi}{N} \sum'_{\lambda\lambda'} |j_\lambda(\mathbf{q})\rangle (\mathbf{J}^{-1})_{\lambda\lambda'} \langle j_{\lambda'}^*(\mathbf{q}) |. \quad (\text{B2})$$

The prime on sums denotes summation such that $l, l' > 0$. The projector Q in Eq. (14) is the given by

$$Q = 1 - P_\rho - P_j. \quad (\text{B3})$$

In order to approximate $M_{\lambda\lambda'}(\mathbf{q}, t)$ Eq. (14) we introduce the projector onto pairs of orientational density modes:

$$\begin{aligned} \mathcal{P} = & \sum_{\substack{\mathbf{q}_1 \mathbf{q}'_1, \mathbf{q}_2 \mathbf{q}'_2 \\ \in 1.\text{BZ}}} \sum'_{\lambda_1 \lambda'_1 \lambda_2 \lambda'_2} |\delta\rho_{\lambda_1}(\mathbf{q}_1) \delta\rho_{\lambda'_1}(\mathbf{q}'_1)\rangle \times \\ & \times g_{\lambda_1 \lambda'_1; \lambda_2 \lambda'_2}(\mathbf{q}_1 \mathbf{q}'_1, \mathbf{q}_2 \mathbf{q}'_2) \langle \delta\rho_{\lambda_2}^*(\mathbf{q}_2) \delta\rho_{\lambda'_2}^*(\mathbf{q}'_2) |, \quad (\text{B4}) \end{aligned}$$

where $(g_{\lambda_1 \lambda'_1; \lambda_2 \lambda'_2}(\mathbf{q}_1 \mathbf{q}'_1; \mathbf{q}_2 \mathbf{q}'_2))$ is the inverse of the static four-point correlation matrix $(\langle \delta\rho_{\lambda_1}^*(\mathbf{q}_1) \delta\rho_{\lambda'_1}^*(\mathbf{q}'_1) \times \delta\rho_{\lambda_2}(\mathbf{q}_2) \delta\rho_{\lambda'_2}(\mathbf{q}'_2) \rangle)$. We use the approximation

$$\begin{aligned} g_{\lambda_1 \lambda'_1; \lambda_2 \lambda'_2}(\mathbf{q}_1 \mathbf{q}'_1, \mathbf{q}_2 \mathbf{q}'_2) \approx & \frac{1}{4} \left(\frac{4\pi}{N} \right)^2 \times \\ & \times \left[\delta_{\mathbf{q}_1 \mathbf{q}_2} \delta_{\mathbf{q}'_1 \mathbf{q}'_2} (\mathbf{S}^{-1}(\mathbf{q}_1))_{\lambda_1 \lambda_2} (\mathbf{S}^{-1}(\mathbf{q}_2))_{\lambda'_1 \lambda'_2} + (1 \leftrightarrow 2) \right], \quad (\text{B5}) \end{aligned}$$

which is consistent with the mode coupling approximation of $M_{\lambda\lambda'}(\mathbf{q}, t)$ for $t = 0$ (see Eq. (B7)).

The mode coupling approximation consists of two main steps. First, the fluctuating force is approximated

$$Q | \mathcal{L} j_\lambda(\mathbf{q}) \rangle \approx \mathcal{P} Q | \mathcal{L} j_\lambda(\mathbf{q}) \rangle. \quad (\text{B6})$$

Substituting (B6) into Eq. (14) leads to a time-dependent four-point correlator, which in a second approximation is

factorized. For $\mathbf{q}_1, \mathbf{q}'_1, \mathbf{q}_2, \mathbf{q}'_2 \in 1.\text{BZ}$ we have

$$\begin{aligned} \langle \delta\rho_{\lambda_1}^*(\mathbf{q}_1) \delta\rho_{\lambda'_1}^*(\mathbf{q}'_1) | Q e^{-iQ\mathcal{L}Q} Q | \delta\rho_{\lambda_2}(\mathbf{q}_2) \delta\rho_{\lambda'_2}(\mathbf{q}'_2) \rangle \approx \\ \frac{N^2}{(4\pi)^2} \left[\delta_{\mathbf{q}_1 \mathbf{q}_2} \delta_{\mathbf{q}'_1 \mathbf{q}'_2} S_{\lambda_1 \lambda_2}(\mathbf{q}_1, t) S_{\lambda'_1 \lambda'_2}(\mathbf{q}_2, t) + (1 \leftrightarrow 2) \right]. \quad (\text{B7}) \end{aligned}$$

With these approximations we obtain

$$\begin{aligned} M_{\lambda\lambda'}(\mathbf{q}, t) \approx & \frac{1}{2} \left(\frac{4\pi}{N} \right)^3 \sum_{\substack{\mathbf{q}_1 \mathbf{q}_2 \\ \in 1.\text{BZ}}} \sum'_{\substack{\lambda_1 \lambda_2 \lambda_3 \lambda_4 \\ \lambda'_1 \lambda'_2 \lambda'_3 \lambda'_4}} \\ & \times \langle (\mathcal{L} j_\lambda(\mathbf{q}))^* | Q | \delta\rho_{\lambda_1}(\mathbf{q}_1) \delta\rho_{\lambda_2}(\mathbf{q}_2) \rangle \times \\ & \times (\mathbf{S}^{-1}(\mathbf{q}_1))_{\lambda_1 \lambda_3} (\mathbf{S}^{-1}(\mathbf{q}_2))_{\lambda_2 \lambda_4} \times \\ & \times S_{\lambda_3 \lambda'_3}(\mathbf{q}_1, t) S_{\lambda_4 \lambda'_4}(\mathbf{q}_2, t) \times \\ & \times (\mathbf{S}^{-1}(\mathbf{q}_1))_{\lambda'_3 \lambda'_1} (\mathbf{S}^{-1}(\mathbf{q}_2))_{\lambda'_4 \lambda'_2} \times \\ & \times \langle \delta\rho_{\lambda'_2}^*(\mathbf{q}_2) \delta\rho_{\lambda'_1}^*(\mathbf{q}_1) | Q | \mathcal{L} j_{\lambda'}(\mathbf{q}) \rangle. \quad (\text{B8}) \end{aligned}$$

APPENDIX C: CALCULATION OF $\langle (\mathcal{L} j_\lambda(\mathbf{q}))^* | Q | \delta\rho_{\lambda_1}(\mathbf{q}_1) \delta\rho_{\lambda_2}(\mathbf{q}_2) \rangle$

This correlator is calculated quite similar to simple [5] and molecular liquids [28, 29, 30] by using Eq. (B3) and $P_j | \delta\rho_{\lambda_1}(\mathbf{q}_1) \delta\rho_{\lambda_2}(\mathbf{q}_2) \rangle = 0$, due to time reversal symmetry. Then we get

$$\begin{aligned} \langle (\mathcal{L} j_\lambda(\mathbf{q}))^* | Q | \delta\rho_{\lambda_1}(\mathbf{q}_1) \delta\rho_{\lambda_2}(\mathbf{q}_2) \rangle = \\ = \langle (\mathcal{L} j_\lambda(\mathbf{q}))^* \delta\rho_{\lambda_1}(\mathbf{q}_1) \delta\rho_{\lambda_2}(\mathbf{q}_2) \rangle \\ - \langle (\mathcal{L} j_\lambda(\mathbf{q}))^* | P_\rho | \delta\rho_{\lambda_1}(\mathbf{q}_1) \delta\rho_{\lambda_2}(\mathbf{q}_2) \rangle. \quad (\text{C1}) \end{aligned}$$

The *first* term on the r.h.s. of Eq. (C1) is easily rewritten by taking into account the hermiticity of \mathcal{L} and the continuity equation Eq. (4) and Eq. (6). This leads to

$$\begin{aligned} \langle (\mathcal{L} j_\lambda(\mathbf{q}))^* \delta\rho_{\lambda_1}(\mathbf{q}_1) \delta\rho_{\lambda_2}(\mathbf{q}_2) \rangle = \\ = \langle j_\lambda^*(\mathbf{q}) j_{\lambda_1}(\mathbf{q}_1) \delta\rho_{\lambda_2}(\mathbf{q}_2) \rangle + (1 \leftrightarrow 2). \quad (\text{C2}) \end{aligned}$$

Substituting the λ -Fourier transform of $\delta\rho_n(\Omega)$ and $j_n(\Omega)$ into the r.h.s of Eq. (C2) we arrive at

$$\begin{aligned} \langle j_\lambda^*(\mathbf{q}) j_{\lambda_1}(\mathbf{q}_1) \delta\rho_{\lambda_2}(\mathbf{q}_2) \rangle &= \frac{N}{4\pi} \frac{kT}{I} \sum_{\mathbf{Q}} \delta_{\mathbf{q}_1+\mathbf{q}_2, \mathbf{q}+\mathbf{Q}} \sum_{\lambda'} i^{l_1+l''-l} (-1)^{m+m''} \left[mm_1 C(ll_1l'', -mm_1 - m'') \right. \\ &\quad - \frac{1}{2} \sqrt{l(l+1) - m(m+1)} \sqrt{l_1(l_1+1) - m_1(m_1+1)} C(ll_1l'', -m-1, m_1+1, -m'') \\ &\quad \left. - \frac{1}{2} \sqrt{l(l+1) - m(m-1)} \sqrt{l_1(l_1+1) - m_1(m_1-1)} C(ll_1l'', -m+1, m_1-1, -m'') \right] c(ll_1l'') S_{\lambda''\lambda_2}(\mathbf{q}_2) \end{aligned} \quad (\text{C3})$$

with

$$c(ll'l'') = \left[\frac{(2l+1)(2l'+1)}{4\pi(2l''+1)} \right]^{\frac{1}{2}} C(ll'l'', 000). \quad (\text{C4})$$

Here we have used the product rule for the spherical harmonics and the factorization of canonic integrals as in Eq. (A2). The *second* term on the r.h.s. of Eq. (C1) is rewritten by using P_ρ from Eq. (B1) and again the hermiticity of \mathcal{L} , as well as the continuity equation:

$$\langle (\mathcal{L}j_\lambda(\mathbf{q}))^* | P_\rho | \delta\rho_{\lambda_1}(\mathbf{q}_1) \delta\rho_{\lambda_2}(\mathbf{q}_2) \rangle = \sum_{\lambda'\lambda''} J_{\lambda\lambda'}(\mathbf{S}^{-1}(\mathbf{q}))_{\lambda'\lambda''} \langle \delta\rho_{\lambda''}^*(\mathbf{q}) \delta\rho_{\lambda_1}(\mathbf{q}_1) \delta\rho_{\lambda_2}(\mathbf{q}_2) \rangle. \quad (\text{C5})$$

Substituting Eqs. (C2), (C3) and (C5) into Eq. (C1), the l.h.s of Eq. (C1) is expressed by the static two-point and three-point correlators $S_{\lambda\lambda'}(\mathbf{q})$ and $\langle \delta\rho_{\lambda''}^*(\mathbf{q}) \delta\rho_{\lambda_1}(\mathbf{q}_1) \delta\rho_{\lambda_2}(\mathbf{q}_2) \rangle$, respectively, and by $J_{\lambda\lambda'}$. $\mathbf{J} = (J_{\lambda\lambda'})$ is calculated in App. A, $\langle \delta\rho_{\lambda''}^*(\mathbf{q}) \delta\rho_{\lambda_1}(\mathbf{q}_1) \delta\rho_{\lambda_2}(\mathbf{q}_2) \rangle$ in App. D.

Now we rewrite $\sum_{\lambda''} \dots$ in Eq. (C3) as follows:

$$\begin{aligned} \sum_{\lambda''} \dots &= \sum_{\lambda''} \sum_{\lambda'_1} i^{l_1+l''-l} (-1)^{m+m''} \left[mm'_1 C(ll'_1l'', -mm'_1 - m'') \right. \\ &\quad - \frac{1}{2} \sqrt{l(l+1) - m(m+1)} \sqrt{l'_1(l'_1+1) - m'_1(m'_1+1)} C(ll'_1l'', -m-1, m'_1+1, -m'') \\ &\quad \left. - \frac{1}{2} \sqrt{l(l+1) - m(m-1)} \sqrt{l'_1(l'_1+1) - m'_1(m'_1-1)} C(ll'_1l'', -m+1, m'_1-1, -m'') \right] \times \\ &\quad \times c(ll'_1l'') \sum_{\lambda''' } (\mathbf{S}^{-1}(\mathbf{q}_1))_{\lambda'_1\lambda'''} S_{\lambda'''\lambda_1}(\mathbf{q}_1) S_{\lambda''\lambda_2}(\mathbf{q}_2), \end{aligned} \quad (\text{C6})$$

and substitute succesively the terms on the r.h.s. of

$$\mathbf{S}^{-1}(\mathbf{q}_1) = \mathbf{d}^{-1} - \mathbf{d}^{-1} + \mathbf{D}^{-1} - \frac{1}{4\pi} \mathbf{c}(\mathbf{q}_1), \quad (\text{C7})$$

which is a rearrangement of the OZ equation (20), into Eq. (C6).

In the first step we replace $d_{\lambda'_1\lambda'''}^{-1} S_{\lambda'''\lambda_1}(\mathbf{q}_1) S_{\lambda''\lambda_2}(\mathbf{q}_2) = d_{\lambda''\lambda_2}^{-1} (d^{-1}S)_{\lambda'_1\lambda_1}(\mathbf{q}_1) (d^{-1}S)_{\lambda_2\lambda_2}(\mathbf{q}_2)$. This expression arises if the matrix elements of \mathbf{d}^{-1} on the r.h.s. of (C7) are used with (C6). Using the explicit result for the matrix \mathbf{d} (see [33]) and the relations

$$\begin{aligned} &\sum_{\lambda''} [mm'_1 c(ll'_1l'') C(ll'_1l'', -mm'_1m'') c(l''l'_2l') C(l''l'_2l', m''m'_2m') \\ &\quad + mm'_2 c(ll'_2l'') C(ll'_2l'', -mm'_2m'') c(l''l'_1l') C(l''l'_1l', m''m'_1m')] \\ &= \sum_{\lambda''} mm'' c(l'_1l'_2l'') C(l'_1l'_2l'', m'_1m'_2m'') c(ll''l') C(ll''l', -mm''m'), \end{aligned} \quad (\text{C8})$$

$$\begin{aligned} &\sum_{\lambda''} [\sqrt{l(l+1) - m(m \mp 1)} \sqrt{l'_1(l'_1+1) - m'_1(m'_1 \mp 1)} c(ll'_1l'') C(ll'_1l'', -m \pm 1, m'_1 \mp 1, m'') c(l''l'_2l') C(l''l'_2l', m''m'_2m') \\ &\quad + \sqrt{l(l+1) - m(m \mp 1)} \sqrt{l'_2(l'_2+1) - m'_2(m'_2 \mp 1)} c(ll'_2l'') C(ll'_2l'', -m \pm 1, m'_2 \mp 1, m'') c(l''l'_1l') C(l''l'_1l', m''m'_1m')] \\ &= \sum_{\lambda''} \sqrt{l(l+1) - m(m \mp 1)} \sqrt{l''(l''+1) - m''(m'' \mp 1)} c(l'_1l'_2l'') C(l'_1l'_2l'', m'_1m'_2m'') c(ll''l') C(ll''l', -m \pm 1, m'' \mp 1, m'), \end{aligned} \quad (\text{C9})$$

we find that this part of (C6) taken together with the same part in the partner expression of (C6) due to (C2) cancels with the part $\langle (\mathcal{L}j_\lambda(\mathbf{q}))^* | P_\rho | \delta\rho_{\lambda_1}(\mathbf{q}_1) \delta\rho_{\lambda_2}(\mathbf{q}_2) \rangle$ of (C1), if Eqs. (D8) and (A4) are used in Eq. (C5).

We turn to the term $\mathbf{D}^{-1} - \mathbf{d}^{-1}$ of (C7), which leads to $(\mathbf{D}^{-1} - \mathbf{d}^{-1})_{\lambda'_1 \lambda'' \lambda_1} S_{\lambda'' \lambda_1}(\mathbf{q}_1)$ if substituted in (C6). Since

$$[D^{-1} - d^{-1}](\Omega, \Omega') = \frac{1}{4\pi} \left[-\frac{1}{4\pi} \frac{1}{\rho^{(1)}(\Omega)} - \frac{1}{4\pi} \frac{1}{\rho^{(1)}(\Omega')} + \frac{1}{(4\pi)^2} \int_{S^2} \frac{1}{\rho^{(1)}(\Omega)} d\Omega \right], \quad (\text{C10})$$

$\mathbf{D}^{-1} - \mathbf{d}^{-1}$ consists just of a nontrivial first row and column, while $\mathbf{S}(\mathbf{q}_1)$ has a vanishing first row and column. So the product $(\mathbf{D}^{-1} - \mathbf{d}^{-1})\mathbf{S}(\mathbf{q}_1)$ has nonvanishing elements in its first row, only. Therefore, $(\mathbf{D}^{-1} - \mathbf{d}^{-1})_{\lambda'_1 \lambda'' \lambda_1} S_{\lambda'' \lambda_1}(\mathbf{q}_1) = 0$, if not $l'_1 = m'_1 = 0$. But if we evaluate the coefficients of (C6) with $l'_1 = m'_1 = 0$, we find that the part $\mathbf{D}^{-1} - \mathbf{d}^{-1}$ of (C7) contributes nothing.

What remains is the last term on the r.h.s. of (C7). If substituted into Eq. (C6) and the corresponding partner expression due to Eq. (C2), respectively, this term delivers the final result

$$\begin{aligned} & \langle (\mathcal{L}j_\lambda(\mathbf{q}))^* | Q | \delta\rho_{\lambda_1}(\mathbf{q}_1) \delta\rho_{\lambda_2}(\mathbf{q}_2) \rangle = \\ & = -\frac{N}{(4\pi)^{\frac{5}{2}}} \frac{kT}{I} \sum_{\mathbf{Q}} \delta_{\mathbf{q}_1 + \mathbf{q}_2, \mathbf{q} + \mathbf{Q}} \sum'_{\lambda'_1 \lambda'_2 \lambda'_3} [b(l'_3 l'_2 l) C(l'_3 l'_2 l, m'_3 m'_2 m) c_{\lambda'_3 \lambda'_1}(\mathbf{q}_1) S_{\lambda'_1 \lambda_1}(\mathbf{q}_1) S_{\lambda'_2 \lambda_2}(\mathbf{q}_2) + (1 \leftrightarrow 2)], \quad (\text{C11}) \end{aligned}$$

with $b(l, l', l'')$ from Eq. (18). Here we have used the relation (A5) for the Clebsch-Gordan-coefficients. If Eq. (C11) and its conjugate is substituted into Eq. (B8) one obtains the mode coupling approximation of the slow part of $M_{\lambda\lambda'}(\mathbf{q}, t)$, which then leads to the final result for $\mathbf{m}(\mathbf{q}, t)$, Eqs. (15)-(19).

APPENDIX D: APPROXIMATION OF

$$\langle \delta\rho_\lambda^*(\mathbf{q}_1) \delta\rho_{\lambda_2}(\mathbf{q}_2) \delta\rho_{\lambda_3}(\mathbf{q}_3) \rangle$$

The approximation of the static three-point correlator is rather involved. Therefore, the most crucial steps are presented only. Readers which are interested in more details are referred to Ref. [40].

The corresponding static three-point-correlator for *simple* liquids was approximated by the convolution approximation [5]. It has been proven that the approximation of the corresponding correlator for molecular liquids [28] is again the convolution approximation as defined in Ref. [50]. However, performing the convolution approximation for molecular crystals does not lead to a simple result. Therefore, we have chosen a different approximation. $\langle \delta\rho_{\lambda_1}^*(\mathbf{q}_1) \delta\rho_{\lambda_2}(\mathbf{q}_2) \delta\rho_{\lambda_3}(\mathbf{q}_3) \rangle$ is the λ -Fourier transform of $\langle \delta\rho_{n_1}(\Omega_1) \delta\rho_{n_2}(\Omega_2) \delta\rho_{n_3}(\Omega_3) \rangle$ given by:

$$\begin{aligned} & \langle \delta\rho_{\lambda_1}^*(\mathbf{q}_1) \delta\rho_{\lambda_2}(\mathbf{q}_2) \delta\rho_{\lambda_3}(\mathbf{q}_3) \rangle = \\ & = \sum_{n_1 n_2 n_3} e^{i(-\mathbf{q}_1 \cdot \mathbf{x}_{n_1} + \mathbf{q}_2 \cdot \mathbf{x}_{n_2} + \mathbf{q}_3 \cdot \mathbf{x}_{n_3})} i^{l_2 + l_3 - l_1} \times \\ & \quad \times \iiint d\Omega_1 d\Omega_2 d\Omega_3 Y_{\lambda_1}^*(\Omega_1) Y_{\lambda_2}(\Omega_2) Y_{\lambda_3}(\Omega_3) \times \\ & \quad \times \langle \delta\rho_{n_1}(\Omega_1) \delta\rho_{n_2}(\Omega_2) \delta\rho_{n_3}(\Omega_3) \rangle. \quad (\text{D1}) \end{aligned}$$

For $\langle \delta\rho_{n_1}(\Omega_1) \delta\rho_{n_2}(\Omega_2) \delta\rho_{n_3}(\Omega_3) \rangle$, one can prove that a

reasonable approximation is

$$\begin{aligned} & \langle \delta\rho_{n_1}(\Omega_1) \delta\rho_{n_2}(\Omega_2) \delta\rho_{n_3}(\Omega_3) \rangle \approx \sum_n \int d\Omega \rho^{(1)}(\Omega) \times \\ & \quad \times \frac{G_{n_1 n}(\Omega_1, \Omega)}{\rho^{(1)}(\Omega)} \frac{G_{n n_2}(\Omega, \Omega_2)}{\rho^{(1)}(\Omega)} \frac{G_{n n_3}(\Omega, \Omega_3)}{\rho^{(1)}(\Omega)}, \quad (\text{D2}) \end{aligned}$$

where $G_{nn_1}(\Omega, \Omega_1) = G_{n_1 n}(\Omega_1, \Omega)$ has been used. Performing the Fourier sums of Eq. (D1) on approximation (D2) yields

$$\begin{aligned} & \frac{N}{(4\pi)^3} \sum_{\mathbf{Q}} \delta_{\mathbf{q}_2 + \mathbf{q}_3, \mathbf{q}_1 + \mathbf{Q}} \int d\Omega \rho^{(1)}(\Omega) \times \\ & \quad \times \frac{S(\mathbf{q}_1, \Omega_1, \Omega)}{\rho^{(1)}(\Omega)} \frac{S(\mathbf{q}_2, \Omega, \Omega_2)}{\rho^{(1)}(\Omega)} \frac{S(\mathbf{q}_3, \Omega, \Omega_3)}{\rho^{(1)}(\Omega)}, \quad (\text{D3}) \end{aligned}$$

where

$$S(\mathbf{q}, \Omega, \Omega') = 4\pi \sum_{\mathbf{x}_{nn'}} G_{nn'}(\Omega, \Omega') e^{i\mathbf{q} \cdot \mathbf{x}_{nn'}}. \quad (\text{D4})$$

Substituting

$$S(\mathbf{q}, \Omega, \Omega') = \sum'_{\lambda\lambda'} (-i)^{l'-l} S_{\lambda\lambda'}(\mathbf{q}) Y_\lambda(\Omega) Y_{\lambda'}^*(\Omega') \quad (\text{D5})$$

and

$$\begin{aligned} & \frac{S(\mathbf{q}, \Omega, \Omega')}{\rho^{(1)}(\Omega)} = 4\pi \int d\Omega'' d^{-1}(\Omega, \Omega'') S(\mathbf{q}, \Omega'', \Omega') = \\ & = 4\pi \sum_\lambda \sum'_{\lambda'} (-i)^{l'-l} (d^{-1}S)_{\lambda\lambda'}(\mathbf{q}) Y_\lambda(\Omega) Y_{\lambda'}^*(\Omega'), \quad (\text{D6}) \end{aligned}$$

with

$$d(\Omega, \Omega') = 4\pi \rho^{(1)}(\Omega) \delta(\Omega|\Omega'), \quad (\text{D7a})$$

$$d^{-1}(\Omega, \Omega') = \frac{1}{4\pi} \frac{\delta(\Omega|\Omega')}{\rho^{(1)}(\Omega)} \quad (\text{D7b})$$

into Eq. (D3) and taking the λ -transforms as defined in Eq. (D1) afterwards we get

$$\begin{aligned} & \langle \delta\rho_{\lambda_1}^*(\mathbf{q}_1) \delta\rho_{\lambda_2}(\mathbf{q}_2) \delta\rho_{\lambda_3}(\mathbf{q}_3) \rangle \approx \\ & \approx \frac{N}{4\pi} \sum_{\mathbf{Q}} \delta_{\mathbf{q}_2+\mathbf{q}_3, \mathbf{q}_1+\mathbf{Q}} \sum_{\lambda'_1} \sum_{\lambda'_2 \lambda'_3} i^{l'_2+l'_3-l'_1} \times \\ & \times c(l'_2 l'_3 l'_1) C(l'_2 l'_3 l'_1, m'_2 m'_3 m'_1) \times \\ & \times S_{\lambda_1 \lambda'_1}(\mathbf{q}_1) (d^{-1}S)_{\lambda_2 \lambda_2}(\mathbf{q}_2) (d^{-1}S)_{\lambda_3 \lambda_3}(\mathbf{q}_3). \quad (\text{D8}) \end{aligned}$$

Although, the product of the last three factors of Eq. (D8) does not look symmetric, one can show that all three factors indeed are equivalent.

-
- [1] *Proc. of 4th International Discussion Meeting on Relaxations in Complex Systems*, eds. K. L. Ngai, G. Floudas, A. K. Rizos and E. Riande, *J. Non-Cryst. Solids*, **307-310** (2001).
- [2] *Special issue: Third Workshop on Non-equilibrium Phenomena in Supercooled Fluids, Glasses and Amorphous Materials*, eds. L. Andreozzi, M. Giordano, D. Leporini and M. Tosi, *J. Phys.: Condens. Matter* **15**, 11 (2003).
- [3] M. Mézard, *Physica A* **306**, 25 (2002).
- [4] U. Bengtzelius, W. Götze and A. Sjölander, *J. Phys. C* **17**, 5915 (1984).
- [5] W. Götze, in *Liquids, Freezing and the Glass Transition*, Proceedings of the Les Houches Summer School of Theoretical Physics, Session LI, 1989, eds. J.-P. Hansen, D. Levesque and J. Zinn-Justin (North-Holland, Amsterdam, 1991).
- [6] R. Schilling, in *Disorder Effects on Relaxational Processes*, eds. R. Richert and A. Blumen (Springer-Verlag, Berlin, 1994).
- [7] W. Götze, *J. Phys.: Condens. Matter* **11**, A1 (1999).
- [8] W. Kob, *J. Phys.: Condens. Matter* **11**, R85 (1999); W. Kob, Les Houches 2002 lecture notes, cond-mat/0212344 (2002).
- [9] K. Binder, J. Baschnagel and W. Paul, *Prog. Polym. Sci.* **28**, 115 (2003).
- [10] R. Schilling, in *Collective Dynamics of Nonlinear and Disordered Systems*, eds. G. Radons, W. Just and P. Häussler (Springer-Verlag, Berlin, 2005); cond-mat/0305565 (2003).
- [11] J. D. Wright, *Molecular Crystals* (Cambridge University Press, Cambridge, 1987).
- [12] *The Plastically Crystalline State*, ed. J. N. Sherwood (Wiley, Chichester, 1979).
- [13] H. Suga and S. Seki, *J. Non-Cryst. Solids* **16**, 171 (1974).
- [14] J. L. Sauvajol, M. Foulon, J. P. Amoureux, J. Lefebvre and M. Descamps, *J. Phys. (Paris)* **43**, supplement no. 12, C9 (1982); M. Descamps and C. Caucheteux, *J. Phys. C* **20**, 5073 (1987).
- [15] R. Brand, P. Lunkenheimer, U. Schneider and A. Loidl, *Phys. Rev. Lett.* **82**, 1951 (1999); R. Brand, P. Lunkenheimer and A. Loidl, *J. Chem. Phys.* **116**, 10386 (2002).
- [16] F. Affouard and M. Descamps, *Phys. Rev. B* **59**, R9011 (1999).
- [17] J. I. Koga and T. Odagaki, *J. Phys. Chemistry B* **104**, 3808 (2000).
- [18] F. Affouard and M. Descamps, in *“Physics of Glasses”*, eds. P. Jund and R. Jullien (AIP, 1999); F. Affouard and M. Descamps, *Phys. Rev. Lett.* **87**, 035501 (2001); F. Affouard, E. Cochon, R. Decressain and M. Descamps, *Europhys. Lett.* **53**, 611 (2001).
- [19] A. Srinivasan, F. J. Bermejo, A. de Andrés, J. Dawidowski, J. Zúñiga and A. Criado, *Phys. Rev. B* **53**, 8172 (1996); M. Jiménez-Ruiz, A. Criado, F. J. Bermejo, G. J. Cuello, F. R. Trouw, R. Fernández-Perea, H. Löwen, C. Cabrillo and H. E. Fischer, *Phys. Rev. Lett.* **83**, 2757 (1999); A. Criado, M. Jiménez-Ruiz, C. Cabrillo, F. J. Bermejo, R. Fernández-Perea, H. E. Fischer and F. R. Trouw, *Phys. Rev. B* **61**, 12082 (2000); A. Criado, M. Jiménez-Ruiz, C. Cabrillo, F. J. Bermejo, M. Grimsditch, H. E. Fischer, S. M. Bennington and R. S. Eccleston, *Phys. Rev. B* **61**, 8778 (2000); M. A. González, E. Enciso, F. J. Bermejo, M. Jiménez-Ruiz and M. Bée, *Phys. Rev. E* **61** 3884 (2000);
- [20] M. A. Ramos, S. Vieira, F. J. Bermejo, J. Dawidowski, H. E. Fischer, H. Schober, M. A. González, C. K. Loong and D. L. Price, *Phys. Rev. Lett.* **78**, 82 (1997); S. Benkhof, A. Kudlik, T. Blochowicz and E. Rössler, *J. Phys.: Condens. Matter* **10**, 8155 (1998); C. Talón, M. A. Ramos, S. Vieira, G. J. Cuello, F. J. Bermejo, A. Criado, M. L. Senent, S. M. Bennington, H. E. Fischer and H. Schober, *Phys. Rev. B* **58**, 745 (1998); H. E. Fischer, F. J. Bermejo, G. J. Cuello, M. T. Fernández-Diáz, J. Dawidowski, M. A. González, H. Schober and M. Jiménez-Ruiz, *Phys. Rev. Lett.* **82**, 1193 (1999); H. E. Fischer, F. J. Bermejo, G. J. Cuello, M. T. Fernández-Diáz, J. Dawidowski, M. Jiménez-Ruiz and H. Schober, *Europhys. Lett.*

- 46**, 643 (1999).
- [21] M. Winterlich, G. Diezemann, H. Zimmermann and R. Böhmer, Phys. Rev. Lett. **91**, 235504 (2003).
- [22] C. Renner, H. Löwen and J.L. Barrat, Phys. Rev. E **52**, 5091 (1995).
- [23] S. Obukhov, D. Kobzev, D. Perchak and M. Rubinstein, J. Physique I **7**, 563 (1997).
- [24] U. T. Höchli, K. Knorr and A. Loidl, Adv. Phys. **39**, 405 (1990).
- [25] K. H. Michel, J. Chem. Phys. **84**, 3451 (1986); Phys. Rev. Lett. **57**, 2188 (1986); Phys. Rev. B **35**, 1405, 1414 (1987); Z. Phys. B **68**, 259 (1987).
- [26] R. M. Lynden-Bell and K. H. Michel, Rev. Mod. Phys. **66**, 721 (1994).
- [27] W. Götze and L. Sjögren, J. Phys. C **17**, 5759 (1984).
- [28] R. Schilling and T. Scheidsteger, Phys. Rev. E **56**, 2932 (1997).
- [29] R. Schilling, Phys. Rev. E **65**, 051206 (2002).
- [30] L. Fabbian, A. Latz, R. Schilling, F. Sciortino, P. Tartaglia and C. Theis, Phys. Rev. E **60**, 5768 (1999).
- [31] D. Forster, *Hydrodynamic Fluctuations, Broken Symmetry and Correlation Functions* (Benjamin, Reading, 1975).
- [32] J. P. Hansen and I. R. McDonald, *Theory of Simple Liquids*, 2nd edition (Academic Press, London, 1986).
- [33] M. Ricker and R. Schilling, Phys. Rev. E **69**, 061105 (2004); cond-mat/0311253 (2003).
- [34] M. Yvinec and R. M. Pick, J. Phys. (Paris) **41**, 1045 (1980); **41**, 1053 (1980).
- [35] W. Breymann and R. M. Pick, Europhys. Lett. **6**, 227 (1988).
- [36] C. Theis and R. Schilling, Phys. Rev. E **60**, 740 (1999).
- [37] C. G. Gray and K. E. Gubbins, *Theory of Molecular Liquids*, vol. I (Clarendon, Oxford, 1984).
- [38] M. Fuchs, W. Götze, I. Hofacker, A. Latz, J. Phys. Cond. Mat. **3**, 5047 (1991).
- [39] M. Letz, R. Schilling and A. Latz, Phys. Rev. E **62**, 5173 (2000).
- [40] M. Ricker, *PhD thesis, Johannes Gutenberg-University, Mainz, Germany* (2004).
- [41] M. Letz and A. Latz, Phys. Rev. E **60**, 5865 (1999).
- [42] A. D. Bruce and R. A. Cowley, Adv. Phys. **29** 1, 111, 219 (1980).
- [43] V. L. Aksenov, M. Bobeth, N. M. Plakida and J. Schreiber, J. Phys. C **20**, 375 (1987); S. Flach and E. Olbrich, Z. Phys. B **85**, 99 (1991); W. Kob and R. Schilling, J. Phys.: Condens. Matter **3**, 9195 (1991); J. Scheipers and W. Schirmacher, Z. Phys. **103**, 547 (1997); R. Schilling, Z. Phys. B **103**, 463 (1997).
- [44] W. Götze and L. Sjögren, Rep. Prog. Phys. **55**, 241 (1992).
- [45] S.-H. Chong and F. Hirata, Phys. Rev. E **58**, 6188 (1998); S.-H. Chong, W. Götze and A. P. Singh, Phys. Rev. E **63**, 011206 (2001).
- [46] W. Götze, in *Amorphous and Liquid Materials*, Vol. 118 of NATO Advanced Study Institute, Series E: Applied Physics, eds. E. Lüscher, G. Fritsch and G. Jacucci (Nijhoff, Dordrecht, 1987); Th. Voigtmann, Phys. Rev. E **68**, 051401 (2003).
- [47] F. Affouard, M. Descamps, cond-mat/0502352 (2005).
- [48] R. Schilling and G. Szamel, Europhys. Lett. **61**, 207 (2003); J. Phys.: Condens. Matter **15**, S967 (2003).
- [49] R. Schilling, in *Advances in Solid State Physics* (Springer-Verlag, Berlin, 2004).
- [50] D. K. Lee, H. W. Jackson and E. Feenberg, Ann. Phys. **44**, 84 (1967).
- [51] Instead, one could also use a complete set of functions, determined by the rotational symmetry. If \mathcal{P} is the point symmetry group of the lattice and \mathcal{P}_M the symmetry group of the molecules, one can use basis functions for irreducible representations of the symmetry group of $\rho^{(1)}(\Omega)$, which is a subgroup of $\mathcal{P} \otimes \mathcal{P}_M$ [26, 34, 35]. For axially symmetric particles, these are linear combinations of the spherical harmonics $Y_\lambda(\Omega)$, $\lambda = (lm)$ [26, 34]
- [52] The static orientational correlators written in complete analogy to simple and molecular liquids are $\mathbf{S}(\mathbf{q}) = [\mathbf{1} - \tilde{\mathbf{D}}^{\frac{1}{2}} \mathbf{c}(\mathbf{q}) \tilde{\mathbf{D}}^{\frac{1}{2}}]^{-1}$, $\tilde{\mathbf{D}} = \frac{1}{4\pi} \mathbf{D}$. This form is equivalent to Eq. (20), but not so handy.
- [53] For $b = 1.1$ we have found the critical $a_c \cong 0.7703$. The corresponding critical NEP are qualitatively very similar to those of Fig. 3. NEP for $a = 1.7$ and $b = 0.66$ are shown in Fig. 12 and discussed in the next paragraph. For fixed $b = 0.66$, $a_c \cong 1.6149$. The corresponding critical NEP are quite similar to those of Fig. 7.
- [54] The simulations in Refs. [16, 18] are performed for a non-rigid lattice, i.e. they include phonons. Therefore, \mathbf{q} is not restricted to the first Brillouin zone and the \mathbf{q} -dependence of the static orientational correlators contain a Debye-Waller factor. As an input into our MCT equations this factor has to be eliminated.